

Theodor Tveit Husefest, Nicolai Andreas Hoel

NTNU
Norwegian University of
Science and Technology
Faculty of Information Technology and Electrical
Engineering
Department of Engineering Cybernetics

Theodor Tveit Husefest
Nicolai Andreas Hoel

Data-Driven Model Predictive Control of Micro-Grid Operation

May 2021



Norwegian University of
Science and Technology

Data-Driven Model Predictive Control of Micro-Grid Operation

Theodor Tveit Husefest
Nicolai Andreas Hoel

Cybernetics and Robotics

Submission date: May 2021

Supervisor: Sebastien Gros

Co-supervisor: Phillip Maree

Norwegian University of Science and Technology
Department of Engineering Cybernetics

Preface

This thesis is the culmination of our master's degree in Cybernetics and Robotics at the Norwegian University of Science and Technology. The work has been done from 04.01.2021 to 31.05.2021 and is a continuation of our project theses. A small part of the code is reused from Theodor Husefest's project work, and the rest is written specifically for this thesis.

We would sincerely like to thank our supervisor at NTNU, Sebastien Gros, for guidance and for helping us overcome our challenges. Furthermore, we would like to thank our industrial supervisor at SINTEF, Phillip Maree, for sharing his time, expertise, and feedback. We could not have done this without your help.

Finally, we would like to thank our family and friends for the support offered during our work.

Abstract

In 2015, 196 countries agreed to the Paris Climate Agreement (*Paris Agreement* 2015), intending to keep global warming below 2°C . Two main measures have to be implemented to reach this goal: more energy production from renewable energy sources and electrification of sectors with high emissions. This transition will lead to a higher demand for electricity and the need for a more efficient operation of the power grid. Micro-grids are distributed power units with internal power production and energy storage, which can increase flexibility in the grid. Micro-grids are therefore suggested as a solution for increasing the use of renewable energy sources and improving the efficiency of the grid.

However, micro-grids are still a field of research. This thesis proposes to develop a model predictive control (MPC) scheme for micro-grids that reflect the economics of being connected to the Norwegian power infrastructure. Furthermore, data-driven prediction methods are developed for forecasting solar production and load demands.

The methods are developed and tested on data from a real-life micro-grid, namely the Skagerak EnergyLab located in Skien, Norway. The micro-grid has a battery energy storage system with a capacity of 1100kWh and PV-cells with a nominal power production of 800kW. It supplies energy to two loads; an industrial facility and a residential neighborhood. A mathematical model was developed and combined with real data measured from the micro-grid to create a realistic simulation environment. The simulations allowed for the testing of the different controllers. Furthermore, keeping the computational time low is considered, as the control system should be able to operate in real-time.

An economic MPC (EMPC) scheme was developed to balance load demands, solar generation, battery storage system, and grid connection in an economical fashion. Furthermore, to handle uncertainty and offer more robust control, the controller was extended to a scenario-tree EMPC (SEMPC) and tested in three configurations; 3, 7, and 9 branches.

Two different prediction methods are proposed for load demands and solar produc-

tion. Load forecasts were implemented with a knowledge-based system. Furthermore, power production from PV cells was calculated with a model found through multiple linear regression, using air temperature and irradiance data from numerical weather forecasts.

The results of the simulations compare the different MPC strategies in the context of computational time and operation cost. Two different models for grid tariff cost are evaluated, the first being the current price model of consumption-based tariff for grid usage. The second is a proposed tariff model by NVE, aiming for a more efficient grid operation where the peak power usage sets the basis for the grid tariff. The baseline used in the results is a rule-based controller, which balances powers without a battery. With the current tariff models, all MPC schemes implemented have similar performance and reduce the total operation cost by 47%. Under the future tariff system of peak cost, the SEMPC with seven branches reduces the operation costs by 55%.

Sammendrag

I 2015 underskrev 196 land klimaavtalen i Paris *Paris Agreement* (2015), med intensjonen om å holde den globale temperaturøkningen under 2 grader. To hovedtiltak som må tas for å nå dette målet er: mer energi produsert fra fornybare kilder og elektrifiseringen av sektorer med høyt utslipp. Denne overgangen vil lede til høyere etterspørsel etter strøm og krever en mer effektiv bruk av strømmettet. Mikronett er distribuerte kraftsystemer med egen kraftproduksjon og energilagring, som kan øke fleksibiliteten i strømmettet. Mikronett er derfor foreslått som en løsning for økt bruk av fornybar energi og effektiv utnyttelse av strømmettet.

Som reguleringsystem i et mikronett foreslår denne oppgaven å bruke modell prediktiv kontroll (MPC) som reflekterer økonomien av å være en del av den norske kraftnettet. I tillegg utvikles metoder for å predikere strømproduksjonen fra et solcelleanlegg og laster som trekker strøm fra mikronettet. Metodene er utviklet og testet med data fra Skagerak EnergyLab i Skien, Norge. Mikronettet har et batterilagringssystem med kapasitet på 1100kWh, og solcellepanel med nominell produksjon på 800kW. Mikronettet leverer strøm til to laster, en industriell bygning og et nabolag. Et realistisk simuleringsmiljø ble utviklet ved å lage en matematisk modell, og data fra mikronettet. Dette ble brukt til å teste forskjellige konfigurasjoner av reguleringsystemet. I tillegg er det lagt fokus på å minimere beregningstiden til systemet, ettersom det skal ha mulighet til å kjøre i sanntid.

En økonomisk MPC (EMPC) ble utviklet for å kontrollere balansering av laster, strømproduksjon fra solceller, batterisystemet og tilkobling til strømmettet på en økonomisk måte. Usikkerheter fra prediksjonsmetodene våre er adressert ved å inkludere mulige scenarioer i reguleringsystemet. Dette ga en senario-tre EMPC (SEMPC), som ble testet i tre konfigurasjoner; med 3, 7, og 9 grener. To forskjellige prediksjonmetoder er foreslått for laster og solcelle-produksjon. Strømforbruket fra lastene blir predikert ved å bruke et kunnskaps-basert system. Produksjonen fra solcellene er beregnet ved å bruke lineær regresjon basert på numeriske værvarsler av solinnstråling og temperatur.

Resultatkapittelet sammenlikninger kostnader og beregningstiden til forskjellige konfigurasjoner av EMPC- strategiene. To forskjellige strukturer for nettleie er testet, hvor den første er den nåværende nettleien med en pris per kWh. Den andre er den nye nettleie-strukturen foreslått av NVE, hvor maksimalt strømforbruk bestemmer nettleien. For å sammenlikne de forskjellige konfigurasjonene brukes et regel-basert reguleringsystem, hvor strømmene er balansert uten bruk av batteriet. Med den nåværende nettleien har alle konfigurasjonene relativt lik ytelse, og kostnadene i systemet er redusert med 47%. Med den nye nettleien er forskjellene større, men systemet med SEMPC reduserer kostnadene med 55%.

Contents

Preface	I
Abstract	IV
Sammendrag	VI
Table of Contents	IX
List of Figures	XII
List of Tables	XIII
Acronyms	XIV
1 Introduction	1
1.1 Skagerak Energylab	1
1.2 Scope	1
1.3 Structure of the Report	3
2 Background and Literature Review	5
2.1 Definitions	5
2.2 Energy Production and Emissions	6
2.3 Norwegian Power Market	7
2.3.1 Spot Market	7
2.3.2 Infrastructure and Effect Based Tariff	8
2.4 Literature Study	11
2.4.1 Model Predictive Control	11
2.4.2 Robust MPC	12
2.4.3 Scenario MPC	13
2.5 Motivation	13
3 Micro-Grids	15
3.1 What is a Micro-grid?	15
3.2 Renewable Energy Sources	16
3.2.1 Photovoltaic Generation	16
3.2.2 Wind Turbines	17
3.3 Load Demands	17
3.4 Energy Storage Systems	17

3.4.1	Flywheels	17
3.4.2	Pumped-Storage Hydro power	18
3.4.3	Batteries	18
3.5	Control Hierarchy	18
4	Time Series Analysis and Forecasting	21
4.1	Evaluation of Time Series Forecasts	22
4.2	Time Series Forecasting Methods	23
4.2.1	Feature-Driven Methods	23
4.2.2	Stochastic Methods	23
4.2.3	Knowledge-Based Methods	24
4.2.4	Mathematical Models	24
5	Model Predictive Control	27
5.1	Dynamic Optimization and Optimal Control Problems	27
5.1.1	Optimal Control	28
5.2	Model Predictive Control	29
5.3	Economic Model Predictive Control	30
5.3.1	Example: Tracking vs. Economic MPC	30
5.3.2	EMPC Stability	31
5.3.3	Dynamic Programming and Terminal Costs	31
5.4	Scenario-Tree MPC	33
5.4.1	Robust and Stochastic MPC	33
5.4.2	Scenario Tree	34
5.4.3	Optimization Problem	35
5.4.4	Approximated Scenario MPC	35
5.5	Numerical Optimization	36
5.5.1	Direct Single Shooting	36
5.5.2	Direct Multiple Shooting	37
6	Methodology	39
6.1	Mathematical Modeling	39
6.1.1	Topology	40
6.1.2	Inputs	40
6.1.3	States and Differential Equation	41
6.1.4	Stage Costs	42
6.1.5	Terminal Cost	43
6.1.6	Optimal Control Problem	44
6.2	Metrics	44
6.2.1	Operational Costs	44
6.2.2	Computational Time	46
6.2.3	Benchmarks	46
6.3	Time Series Analysis	46
6.3.1	Data Cleaning	46
6.3.2	Photovoltaic Forecasting	48
6.3.3	Load Forecasting	53

6.4	Handling Uncertainty	55
6.4.1	Scenario-tree EMPC	55
6.4.2	Selecting Scenarios	57
6.5	Methodology Summary	62
7	Results	63
7.1	Experiment 1 - Terminal Cost	63
7.2	Experiment 2 - Fixed Tariff	66
7.2.1	Experiment 2.1 - Fixed Tariff, Perfect Predictions	66
7.2.2	Experiment 2.2 - Uncertainties	68
7.3	Experiment 3 - Effect Based Tariff	71
7.3.1	Experiment 3.1 - Perfect Predictions	71
7.3.2	Experiment 3.2 - Uncertainties	71
8	Discussion	77
8.1	Forecasting	77
8.2	The Value of EMPC in Skagerak Energylab	78
8.3	Uncertainties	79
9	Conclusion	81
9.1	Further work	82
	References	83
A	Appendix	89
A.1	Software and Solver	89
A.1.1	Interior Points methods	89
A.1.2	Line Search	90
A.1.3	Filters	90

List of Figures

1.1	Topology of Skagerak Energylab.	2
2.1	Power production by sources	7
2.2	Emissions from Norwegian territory	8
2.3	Bidding zones	9
3.1	General micro-grid control hierarchy.	19
5.1	Economic MPC and tracking MPC illustrated	31
5.2	Scenario tree illustration	34
6.1	System architecture	40
6.2	Simplified topology of Skagerak Energylab.	41
6.3	Photovoltaic power measured from April 10th to April 17th	47
6.4	Feature correlation matrix	49
6.5	Auto-correlation on PV signals	49
6.6	Illustration of the prediction pipeline	50
6.7	Example of Solcast forecast	50
6.8	Weighting of prediction and measurements	52
6.9	Load demand from April 7th to April 17th	53
6.10	Auto-correlation of load time-series	54
6.11	Kernel density estimate	56
6.12	PV and load prediction scenarios	59
6.13	Kernel density estimation with optimistic and pessimistic scenarios	60
6.14	Standard deviation for PV and load uncertainty	61
7.1	SOC - Terminal cost comparison	65
7.2	Experiment 2.1 - from April 7th to April 9th	67
7.3	Experiment 2.2 - from April 15th to April 16th	69
7.4	Predicted and observed values of PV and load on 15. April	70
7.5	Experiment 3.1 - from April 7th to April 9th	72
7.6	Comparison of peak power from April 7th to May 7th.	73

7.7	Experiment 3.2 - SOC comparison	74
7.8	Plot of recourse action/primary controls effect on peak power	74

List of Tables

4.1	PV model parameters	25
6.1	Relevant Time Series	47
6.2	Root mean squared error of numerical weather forecasts	51
6.3	Root mean squared error of MLR and mathematical PV-model	51
6.4	Root mean squared error of PV predictions with linear mixture	52
6.5	Root mean squared error of PV predictions with linear mixture	54
7.1	Parameters used in experiments	64
7.2	Performance comparison with terminal cost	65
7.3	Benchmarks for fixed grid tariff.	66
7.4	Performance comparison with fixed grid tariff	70
7.5	Benchmarks with effect-based tariff	71
7.6	Performance comparison with effect-based tariff	75

Acronyms

1-RMSE One-Step Root Mean Squared Error

A-RMSE Average Root Mean Squared Error

ANN Artificial Neural Network

AR Auto-Regressive

ARIMA Auto-Regressive Integrated Moving Average

ARMA Auto-Regressive Moving Average

AT Air Temperature

CINELDI Centre For Intelligent Electricity Distribution

DEMPC Deterministic Economic Model Predictive Control

DEMPC-PP Deterministic Economic Model Predictive Control with Perfect Predictions

EMPC Economic Model Predictive Control

EMS Energy Management System

ESS Energy Storage System

GHI Global Horizontal Irradiance

IP Integer Programming

KDE Kernel Density Estimation

LP Linear Programming

MA Moving Average

MIP Mixed Integer Programming

MLP Multiple Linear Regression
MPC Model Predictive Control
NLP Nonlinear Programming
NWP Numerical Weather Predictions
OCP Optimal Control Problem
ODE Ordinary Differential Equation
PAI Plane of Array Irradiance
PSH Pumped-Storage Hydro
PV Photovoltaic
QP Quadratic Programming
RES Renewable Energy Sources
RMSE Root Mean Squared Error
RTO Real-Time Optimization
SARIMA Seasonal Auto-Regressive Integrated Moving Average
SEMPC Scenario-tree Economic Model Predictive Control
SOC State Of Charge
SQP Sequential Quadratic Programming
TS Time Series
TSO Transmission System Operator

Introduction

1.1 Skagerak Energylab

This master thesis is written in cooperation with *Centre for Intelligent Electricity Distribution* (CINELDI), which is one of the *Centers for Environment-friendly Research*. The goal of CINELDI; *enable a cost-efficient realisation of the future flexible and robust power-grid* (CINELDI 2020). As a part of this, the micro-grid Skagerak EnergyLab has been created for research purposes.

The Skagerak Energylab is located in Skien, Norway, at the football stadium Skagerak Arena. The stadium's roof is covered with 4300 square meters of photovoltaic cells, which have a nominal peak power of 800kW. Furthermore, it has a battery system with 1100kWh storage capacity and a maximum power dispatch of 800kW. The micro-grid is responsible for supplying energy to both the stadium and a local residential area. Also, as a micro-grid, it can operate in both island and grid-connected modes. An illustration of the micro-grid topology is shown in Figure 1.1.

1.2 Scope

This thesis is centered around a case study of a real micro-grid, where model predictive control (MPC) and data-driven prediction methods are tested to increase the economic performance of the micro-grid. A mathematical model of the system is developed and combined with real data collected from the micro-grid to create a realistic simulation environment. The simulations allowed for the testing of the different controllers.

By collecting data and running experiments on the micro-grid, the goal is to better understand the interaction between solar power generation, battery storage

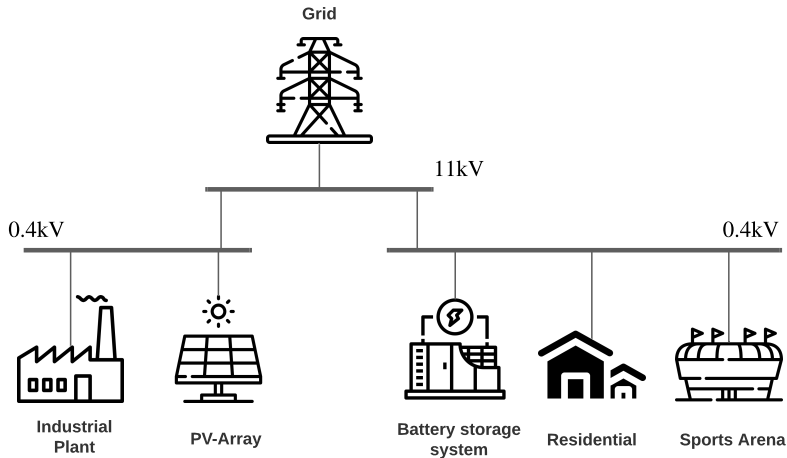


Figure 1.1: Topology of Skagerak Energylab.

systems, and the interaction with the existing power grid.

An economic MPC (EMPC) scheme is developed to balance load demands, solar generation, battery storage system, and grid connection in an economical fashion. By comparing the performance of the EMPC with a no-battery controller, the value of proper scheduling and efficient use of the battery is investigated. The intermittent nature of solar production and load demands make predictions difficult, and some uncertainty can be expected. To handle this uncertainty and offer robust control, a scenario-tree EMPC (SEMPC) is developed and tested in three configurations; 3, 7, and 9 branches.

The data-driven methods proposed in this thesis are used to create better predictions of load consumption profiles and PV production. Different methods have been examined based on the accuracy of the predictions and computational efficiency. Load forecasts are implemented with a knowledge-based system. Furthermore, power production from PV cells are calculated with a model found through Multiple Linear Regression and irradiance data based on numerical weather forecasts.

The main research questions addressed in this thesis are listed below:

1. Which methods should be used to efficiently forecast solar production and load demands?
2. What is the value of using an EMPC-scheme as an energy management system

at the Skagerak EnergyLab in contrast to more rule-based control strategies?

3. What are the consequences of uncertainties in the EMPC-scheme, and can a robust/stochastic formulation increase the performance?

1.3 Structure of the Report

This thesis is organised in the following way.

1. Chapter 1 - *Introduction*, outlines the background and scope for the thesis.
2. Chapter 2 - *Background*, gives an overview of the Norwegian energy market and a literature review of the different MPC-schemes.
3. Chapter 3 - *Micro-grids*, introduces the concept of micro-grids.
4. Chapter 4 - *Time-series Analysis and Forecasting*, presents and compares the different methods for predictions.
5. Chapter 5 - *Model Predictive Control*, introduces the concept of different model predictive control methods.
6. Chapter 6 - *Methodology*, presents the methods used in this thesis.
7. Chapter 7 - *Results*, presents the results of this thesis.
8. Chapter 8 - *Discussion*, reflects around the methods and results presented in the thesis.
9. Chapter 9 - *Conclusion and further work*, concludes the work with a summary and suggestions for further work.

Background and Literature Review

In this chapter, the contextual background for this thesis is offered. The test system for the performed case-study is located in Norway, and the main focus will be on the Norwegian power market and emissions.

First, a few commonly used terms from the micro-grid literature are defined. Next, the differences in energy production in Norway and globally are presented. Then follows an introduction to the transmission grid in Norway and the potential economical changes it faces. Next, a technical literature study on the field of model predictive control in micro-grid. Finally, the chapter is summarized by stating the motivation for the thesis.

2.1 Definitions

- *Effect-based tariff* - The proposed new model where the grid tariff is based on the maximum power drawn from the grid in a month.
- *Fixed grid tariff* - The current consumption-based grid tariff that has a fixed price per kWh.
- *Grid-connected mode* - The micro-grid is connected to the main power grid and can trade power at certain tariffs. When connected, the main grid is responsible for primary control.
- *Islanded mode* - The micro-grid is disconnected from the main grid, and operates individually with local control.
- *Loads* - Energy drawn from the micro-grid to the consumer. If the micro-grid has control over a load, such as a possibility of charging an electric car, the load is called controllable. In this thesis, all loads are non-controllable, so the power demanded has to be provided at all times.

- *Power balance* - All power systems, for example, a power grid, must have an equal amount of power supply and power demand at all times. If the power system is unbalanced, it results in unwanted effects on the power quality and frequency.
- *Predictions/forecasts* - The estimated future value of signals or parameters. The most used examples in this thesis are power generated from photovoltaic cells and load demands.
- *Primary control* - Control layer handling power quality and stability. Primary control usually operates on a resolution of seconds to minutes.
- *Secondary control* - Often called *energy management system* (EMS). The economical layer of control, responsible for reducing the stress for primary control. Usually operates on a resolution of hours to days.
- *Uncertainties* - Random variables that can be described by a probability distribution.

2.2 Energy Production and Emissions

Norway has a unique position in energy production due to the high mountains and wet climate that facilitates hydropower production. Figure 2.1 illustrates the fraction of different energy sources used for power production in Norway compared to the rest of the world. From March 2020 - March 2021, 100% of the national power production came from renewable energy sources (RES), and hydro accounts for 89.8% of all production (Statistics 2020). However, on a global scale, this is not the case. Only 29% of electricity produced in the world originates from RES.¹ However, if the goal of keeping the rise in world temperature below 2 °C should be reached (*Paris Agreement* 2015), energy production from RES has to increase significantly. In addition, hydropower is limited to a few countries like Norway. Removing hydropower, the two main RES left are solar and wind (SW). Although SW are increasing globally (Ritchie 2021), there are challenges when incorporating them into the existing power grid.

One of the main tasks of the power grid is to make sure the power balance is maintained. This entails that electricity produced should be equal to electricity consumed at any given time and is discussed further in Chapter 2.3. Fossil-fueled power production has the advantage that it is possible to increase production as demand increase. SW, however, relies on the weather, and the excess energy under high production has to be stored so it can be used when the load demands it.

Even though all electricity production in Norway is from RES, there are still emissions. Figure 2.2 shows which sectors that are responsible for the emissions in Norway. The oil and gas extraction and industry are together accountable for

¹Note: Nuclear production is left out as this is a different discussion.

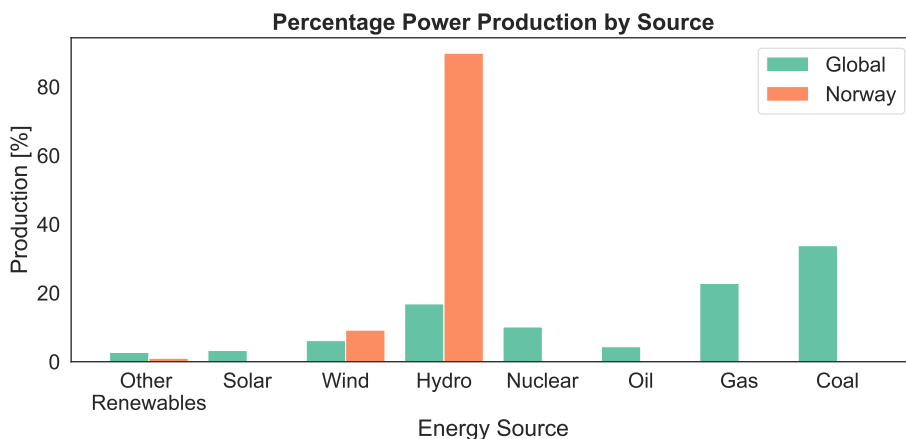


Figure 2.1: Percentage energy production in Norway vs. globally. Collected from Statistics Norway (Statistics 2021) and Our World in Data. (Ritchie 2021)

over 50% of emissions, followed by transportation with ca. 31% (Statistics 2021). To reduce the emissions in these sectors, they need to be *electrified*. Electrification means switching from technology and services that rely on fossil fuels to electricity. For example, changing from a diesel to an electric vehicle.

2.3 Norwegian Power Market

As discussed in the previous section, Norway’s power production is mainly hydropower. This gives Norway some of the lowest electricity prices in Europe. Today, the electricity prices are divided into five bidding zones in Norway, which means the prices can vary from area to area. The bidding zones are made to reflect the transmission capacities between areas of production and consumption. Bottlenecks in the transmission capacity cause different prices. For example, suppose a power producer can supply cheap power in northern Norway. In that case, this will be of little help to power demand in southern Norway if there is not enough capacity to transmit it from producer to consumer.

2.3.1 Spot Market

The electricity bidding market is managed through NordPool ², a shared electrical market for all of northern Europe. A day before the production hours, the day-ahead market, also known as the spot market, holds an auction where bids are based on the predicted load demand. This auction sets the schedule and the power

²<https://www.nordpoolgroup.com/>

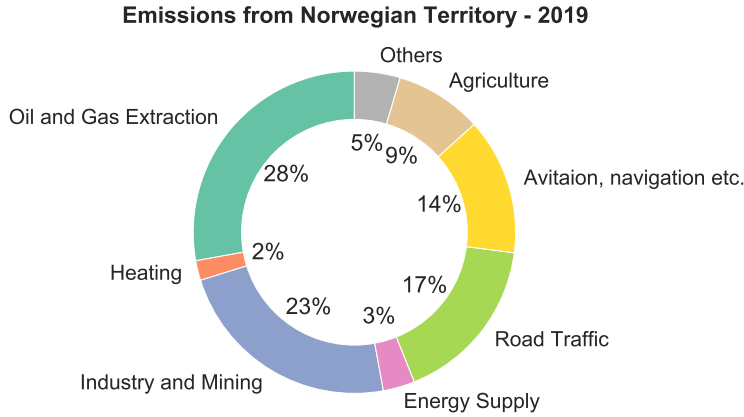


Figure 2.2: Percentage emissions in CO_2 -equivalents from Norway in 2019. Collected from Statistics Norway (Statistics 2021)

price for the next day. Closer to the hour of production, the intraday market allows further trading to correct imbalances. In the last hour before production, the balancing market tries to fix the previous imbalances between production and demand. In the balancing market, power producers can give bids for flexibility, where they offer possible up- or down-regulation of the power production. This regulation is handled by the transmission system operator (TSO), which buys reserve power to ensure the instantaneous power balance at all times.

2.3.2 Infrastructure and Effect Based Tariff

This section is based on the comprehensive report ³ ordered by *The Norwegian Water Resources and Energy Directorate* (NVE) on the current changes in the Norwegian power market, and specifically how the electrical infrastructure is financed.

The Norwegian transmission grid is part of a Nordic synchronous area that shares a standard frequency, including Sweden, Finland, and parts of Denmark. This area has common frequency control and power balancing. The TSO handles the power balance. In Norway and the Nordic area, the TSO is Statnett with support from Svenska kraftnät. Statnett also owns the central transmission grid in Norway, which delivers electricity between regions. The regional transmission grids are regulated such that private companies can own them, but only a single company can operate in a given area (Regjeringen.no 2016). As this induces a monopoly, the companies owning the grid are forbidden to profit and only collect

³URL: https://publikasjoner.nve.no/rme_hoeringsdokument/2020/rme_hoeringsdokument2020_01.pdf

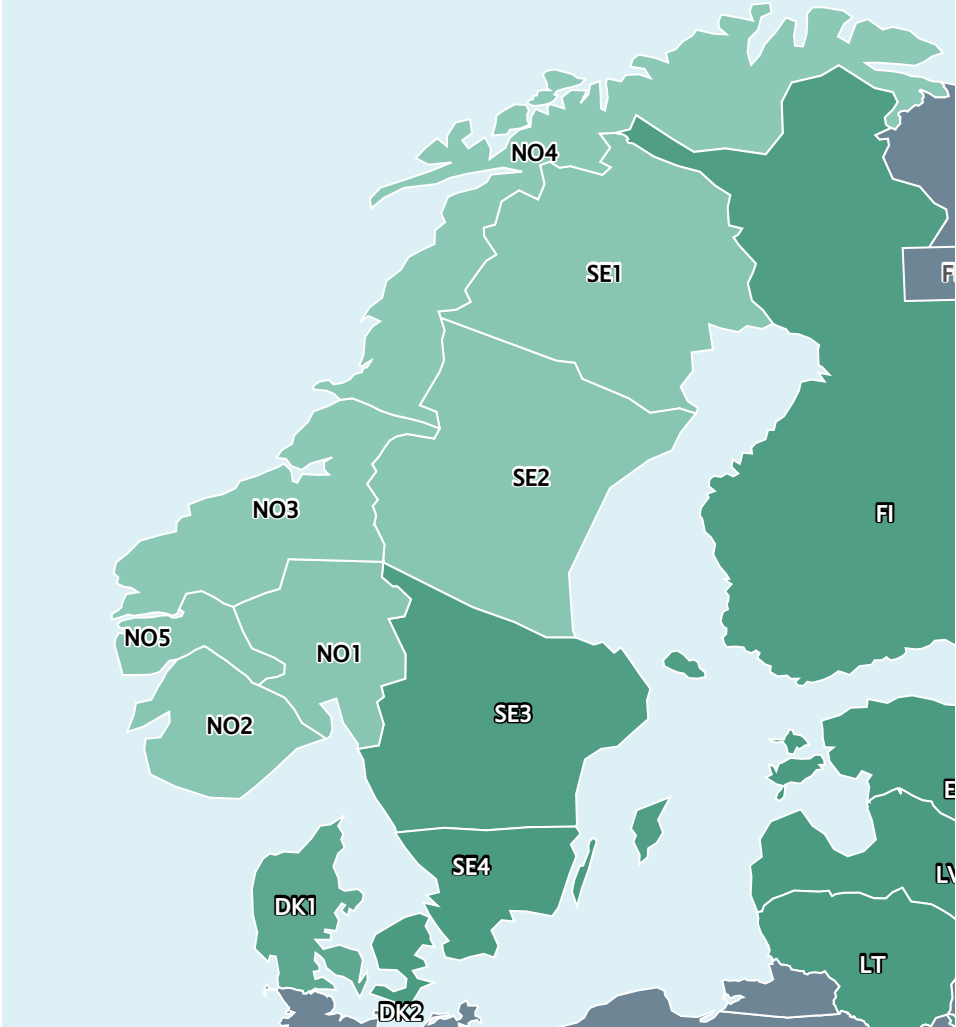


Figure 2.3: Bidding zones for electrical spot prices.

fees to cover expenses associated with the transmission grid.

The current tariff system has two components. One is constant and is a payment for being connected to the grid, and the other is a fixed cost for the amount of energy bought, measured in kWh. However, the way we use energy is changing. As a measure to reduce greenhouse gas emissions, several sectors of society are getting electrified. The transition leads to higher consumption of electricity, as well as new ways to utilize the power. For example, over half of the private cars sold in 2020 in Norway were electric, according to *Statistics Norway* (Andresen 2021). Although this is good in an environmental setting, it is raising challenges for the transmission grid, especially during *peak-hours*. These are hours where the most power is drawn from the grid and usually occurs in the morning as people wake up and in the afternoon when people get home from work.

The costs of the transmission grid can be separated into two components. The first is *transmission loss*, which are energy losses that occur as electricity is transported from production to consumer. The losses are caused by electrical resistance⁴ in the transmission lines, following the definition of electrical power

$$P = VI \tag{2.1}$$

By inserting Ohms law

$$V = IR, \tag{2.2}$$

and the resistance of the transmission line R_{trans} we get

$$P_{loss} = I^2 R_{trans} \tag{2.3}$$

The losses increase with the square of the current, which is compensated in the transmission grid by having high voltage. However, as the demands for electrical power increase, the current has to increase, and therefore as a consequence the transmission losses also increase.

The other costs are related to grid capacity, either via investments or maintenance, and are responsible for 80-90% of all expenses. The main challenges occur in peak hours when the maximum energy is drawn from the grid. As the transmission lines have a maximum capacity, they are continuously upgraded to keep up with the increasing energy demand. However, in the off-peak hours, much of the capacity is not being utilized.

Due to the described capacity situation, NVE is looking into the possibilities of changing the grid fee to reflect these changes and give incentives to use the transmission grid more effectively. The new fee is called *effect-based tariff* and will, if implemented, replace the current fixed price model. Instead of measuring the amount of energy used, the fee is determined by the peak power, which is the maximum energy drawn from the grid. As a customer, it will be economically

⁴Some losses also come from impedance. However, this is neglected in this thesis.

beneficial to spread the power consumption throughout the day, for example, by charging the electric car during the night. The intention behind effect-based tariffs is to reduce transmission losses and minimize the need for investments in the future.

2.4 Literature Study

This section is meant to introduce Model Predictive Control (MPC) as a control method for micro-grid operation. Some topics are more advanced and will be explained in detail later in the thesis.

2.4.1 Model Predictive Control

The method of model predictive control (MPC) is widely studied and applied in the industry (Qin & Badgwell 2003). Model predictive control for micro-grids has been researched, and several case studies have been conducted Parisio et al. (2014), Shan et al. (2018). The goal of the controllers is to balance power and load in the micro-grid, which is done by stabilizing the system model and satisfying constraints. The papers presented in this section use a special case of MPC called economic MPC, where the objective functions seek to maximize the economic profit/ minimize the costs of a micro-grid.

In their paper, Clarke et al. (2016) simulate an MPC on a micro-grid model with several different production units. The controller's goal is to minimize the operation cost while keeping the system within safety limits. The paper shows that the controller is successful in this goal, and the article also indicates that increasing the resolution of the MPC can lead to higher profit. The resolution is increased from 60 to 5 minutes, which results in a consistent decrease in the operational cost of the micro-grid. This is mainly due to fluctuations in solar power production, and by decreasing the sampling time, the controller can better react to changes in the system.

When there are several loads and production units in the grid, a unit commitment problem can be formulated to assert which units are supposed to be online. For example, if the power capacity cannot meet the load demand, shedding non-essential loads is a unit commitment problem. Another example is whether to start up extra generators or curtail power production. This problem is discussed in Novickij & Joos (2019) where the authors try to tackle the unit commitment problem by decoupling from the economic problem and running a two-stage MPC that handles each of the subproblems separately. The proposed two-stage method is compared to a single-stage MPC and gives a lower computationally cost. Lower computationally cost allows for shorter time steps in the MPC. Clarke et al. (2016) presents how this can provide a decrease in operation cost by reacting more quickly to changes in the system.

In Patiño et al. (2014), the MPC objective function is not purely economic. The paper adds a tracking term that penalizes deviations in the battery state of charge from a reference value. The reference value is chosen at 50% of max capacity, where the battery can absorb or feed in extra power to the micro-grid. The tracking term is implemented to avoid depletion of the battery at the end of each prediction horizon, which is a consequence of having no terminal cost in the objective function. It also adds a penalty term for the difference in actuator usage from one time step to the next. This term helps avoid sudden and abrupt usage patterns of the grid and the battery, decreasing the wear and increasing safety margins. However, both these terms come with a trade-off with economic performance. The results show that the MPC-controlled EMS effectively meets the load demands at all times.

2.4.2 Robust MPC

Most systems include some uncertainty, either through model-plant-mismatch or due to external stochastic disturbances in the system. A grid-connected micro-grid faces no severe consequences from breaking the battery constraints since it can utilize the grid to solve the problem. A micro-grid either in island mode or has a higher peak demand than the central grid's transmission lines can supply potentially faces a blackout if the battery is emptied. Other systems can have much more severe consequences from constraint violation. To deal with dangerous constraint violation and uncertainty, a controller that can guarantee the constraints is needed. For this purpose, a robust MPC is proposed. In robust MPC, an early contender is the min-max MPC that plans the optimal solution based on the worst-case scenario realization of the uncertainty.

In Carli et al. (2020) a robust MPC is proposed for a micro-grid with both electrical and thermal loads. The system is modeled with a box-uncertainty set which accounts for each uncertainty parameter independently. The robust MPC seeks to safeguard itself from the worst-case realization of the uncertainty in the system. This means that the solution tries to be feasible for any realization of the uncertainty set. The paper also presents a way to tune the robustness of the MPC. It does so by having weights on the predictions and the worst-case scenario. Giving the predictions full trust results in a deterministic MPC while weighing the worst-case scenario gives a min-max MPC. The weights allow tuning of the controller to find an MPC scheme somewhere in between. The paper compares a robust MPC scheme with a deterministic MPC and shows that the number of times the controller breaks the constraints drops quickly as the robustness of the system increases. Over a thousand simulations, the percentage of infeasible solutions is 34% for a deterministic MPC and 0% for the fully robust MPC. This advantage comes at a cost, and the robust MPC has an operational cost about twice as high as the nominal MPC.

In the paper by Zhou et al. (2016), the authors compares a min-max MPC to a certainty equivalent MPC on a micro-grid. The certainty equivalent MPC takes the probability averaged mean of the forecast and uses that value as the predic-

tion. The results here are similar to what can be seen in other papers, i.e the robust min-max method decreases constraint violations but increases cost due to its conservative solutions.

2.4.3 Scenario MPC

Robust MPC schemes can be very conservative and often sub-optimal in the optimization of the objective function. This is due to the focus on worst-case scenarios. A more recent implementation of min-max MPC has been studied in scenario-tree MPC (SMPC), also called feedback min-max MPC. The SMPC models the different realizations of the uncertainty through branches of possible realizations and optimizes across them. Since it is numerically impossible to model all possible realizations, this technique relies on efficiently choosing the scenarios.

Scenario trees that try to span the entire uncertainty set, faces difficulties when there is more than one uncertainty parameter. A method that builds branches with all combinations of the maximum and minimum values for all the parameters might cover highly unlikely or impossible scenarios. As shown in Krishnamoorthy, Thombre, Skogestad & Jäschke (2018), the likelihood of an extreme value in all the uncertainty parameters is quite unlikely. The authors propose a method where a principal component analysis reveals the correlation and variance of the data and reduces the size of the uncertainty set.

In Hans et al. (2015) a scenario-based solution is implemented to handle uncertainty in an islanded micro-grid. The paper first uses Monte Carlo simulations to represent the probability distribution of the uncertainty. Then a method called the forward selection algorithm is used to create the scenario tree. A scenario-tree MPC is compared to an MPC with perfect prediction and a min-max MPC. The scenario-tree MPC has a lower operational cost than the min-max MPC but also more constraint violations.

2.5 Motivation

The motivation behind this thesis summarizes the topics that have been discussed so far. Chapter 2.2 shows that the global use of renewable energy sources has to increase, as well as the challenges associated with solar and wind power generation. Forecasting power production from solar and wind and using electricity storage effectively is necessary to incorporate them into the existing power grid. Furthermore, sectors with high emissions of greenhouse gasses are getting electrified, which is straining the infrastructure that distributes electricity. Therefore, the grid has to be used more efficiently to reduce losses and limit investments. To give incentive to the customers of the power grid, Norwegian authorities (NVE 2018) has proposed to change to an effect-based tariff. Micro-grids offer flexibility with energy storage

systems and distributed energy generation. This thesis aims to research a controller that takes advantage of this flexibility, reduces electricity cost, and accommodates the uncertainty introduced by intermittent RES generation.

The overall objective issued by Skagerak EnergyLab and SINTEF CINELDI is to reduce the cost of a micro-grid operation. However, doing this entails creating solutions that incorporate solar power production and is a part of the modern Norwegian power grid. This, again, can lead to reduced emissions. Based on literature (Chapter 2.4), Economic Model Predictive Control (EMPC) is believed to be a good solution for an energy management system.

Chapter 3

Micro-Grids

So far, the challenges with renewable energy sources and power transmission have been discussed and micro-grids as a possible solution was presented. This chapter by elaborating on micro-grids and their position in the transmission grid. Then the central components of a micro-grid are discussed, namely renewable energy sources, loads, and energy storage systems. The chapter ends by describing the control hierarchy of a micro-grid and which layer of control is of interest in this thesis.

3.1 What is a Micro-grid?

Micro-grids have to some degree been around for a long time, but have recently gained attention as a component of the green shift (Marnay et al. 2015). As discussed in Chapter 2.2, energy production from renewable energy sources (RES) is expected to grow. RES has a relatively low production capacity per square kilometer compared to traditional power plants running on fossil fuel. Furthermore, coal, gas, and oil are easy to transport, which means that fossil energy plants can be placed almost anywhere. Large, centralized power plants can supply large areas with electricity, which has led to a top-down design of the power grid. In contrast, RES depends on local weather conditions for optimal power production and cannot be placed arbitrarily. Utilizing RES are therefore leading to more distributed energy production, which offer challenges when incorporated into the existing power grid.

Micro-grids appear at different scales and with different configurations of components. The CIGRÉ Work Group (Marnay et al. 2015) offers the following definition:

Micro-grids are electricity distribution systems containing loads and distributed energy resources, (such as distributed generators, storage de-

vices, or controllable loads) that can be operated in a controlled, coordinated way either while connected to the main power network or while islanded.

Distributed energy production also leads to *prosumers*, who are customers who both buy and sell electricity back into the grid. This bidirectional power flow is difficult to control centrally, and therefore micro-grids are used as a buffer, providing decentralized control. If the distributed production can be bundled together with local loads into micro-grids and controlled locally, the micro-grid can act as a singular unit connected to the grid.

Another challenge with renewable energy is the intermittency and its effect on the power balance of the grid. Production is not controllable and does not necessarily align with the demand. Local energy storage systems (ESS) can alleviate these problems. ESS can mitigate the variable production by supplying power when the demand exceeds the production and store energy when production exceeds demand. For the micro-grid to solve these problems, it needs a controller to properly schedule power trade with the main grid and predict load demand and RES.

Marnay et al. (2015) summarizes this into three main benefits of using micro-grids:

- To better utilize local assets which are difficult to incorporate into the main grid. Relevant assets are small-scale RES for power production or electric vehicles as batteries.
- Provide high-quality power and reliability to local services. This is relevant in areas with poor infrastructure or if the micro-grid is supplying emergency services.
- Providing a controlled profile to the wider power system, e.g., damping the variability of local renewable resources and loads.

3.2 Renewable Energy Sources

This section introduces the most commonly used renewable energy sources.

3.2.1 Photovoltaic Generation

Photovoltaic (PV) cells collect energy from the photons coming from the sun. A typical cell comprises a semiconductor material, most commonly silicon, with a positive and a negative doped side. Doped in this context means adding small amounts of atoms of another element that change the material's electron balance. The positive side lacks electrons, and the opposing side has an excess. Between the two layers is a diode allowing one-way travel for electrons. If hit by a photon, the electrons absorb the energy of the photons and detach from their atoms. The

electrons can then travel through the diode, which causes a difference in the voltage between the layers used for electrical work. The photons must be in the suitable energy range for the electrons to absorb the photon's energy. The energy range is determined by the position of the electron in the atom.

3.2.2 Wind Turbines

Wind turbines generate power by harvesting the kinetic energy from the wind. A wind turbine has rotor blades that are propelled by the pressure difference around the blades. There is a maximum percentage of the power that can be produced, which is called the Betz limit and is 53.9%. Intuitively, the limit comes from removing the kinetic energy from the wind, slows, or stops the air movement. Therefore there is a limit to how much the wind can be slowed before it starts to accumulate and build up pressure behind the wind turbine. Even though wind turbines are the second-fastest-growing RES, they are not a component in the Skagerak Energylab and will therefore not be discussed further in the thesis.

3.3 Load Demands

The goal of a power system is to transmit power from energy production to demand. A load can be an industrial plant, a private household, or anything running on electrical power inside the micro-grid. The loads in the micro-grid are often combined into a single load since this assumption simplifies the system model. The load can be split into two categories, controllable and critical/non-controllable loads (Cominesi et al. 2018). Controllable loads can safely turn off without the risk of lives or significant economic losses. If the total load exceeds the power in the system, it runs the risk of a blackout if there is no backup power. To avoid a blackout, the system can turn off or shed controllable loads. In this thesis, it is assumed that all loads are critical and load shedding will therefore not be discussed any further.

3.4 Energy Storage Systems

An energy storage system is responsible for coordinating the different types of energy storage in a micro-grid and handle charging/discharging of them. The ESS can include several energy-storing components, each with its advantages and disadvantages. Storage methods with large capacity like hydro pumps are slower to come online and deliver power. In contrast, storage methods with smaller capacity like flywheels have a low reaction time and can stabilize the power balance for a short time and avoid grid failure while the slower storage types come online (Rahman et al. (2020)).

3.4.1 Flywheels

Flywheels stores energy as rotational energy. As the name implies, it is made up of a spinning wheel that can quickly be accelerated or decelerated. When there

is a sudden need for power in the system, flywheels can quickly be decelerated to generate power. Though the wheels' tensile strength limits the amount of energy stored, flywheels have many advantages over other storage forms. It can operate in a larger temperature range than batteries, the amount of energy stored can easily be measured via the rotational speed ω , (3.1), and the flywheel has a very long lifespan (Khodadoost Arani & Gharehpetian 2014), (Bordons et al. 2020).

$$\frac{1}{2} * J_m * \omega^2 \tag{3.1}$$

3.4.2 Pumped-Storage Hydro power

Pumped-Storage Hydro (PSH) is a method for storing large amounts of energy. If there is an excess of electricity in the power system, a motor pumps water from a lower reservoir to an upper reservoir higher in altitude. When energy is needed, the pump turns into a regular hydropower plant. The water's potential energy at the upper reservoir is turned into kinetic energy used in a turbine to generate power. This method store a large amount of energy, but it takes time to both fill the storage and discharge it (Chen et al. (2009)). The main problem with PSH is that it is dependent on a significant drop in altitude and is therefore limited to a small number of areas.

3.4.3 Batteries

Batteries represent a trade-off, with a medium response and medium storage size. In this thesis, the ESS will only consist of a single battery to accurately portrait the case study. There are many types of batteries, though lithium-ion batteries are the most common. All batteries experience some form of degradation, and it happens over time for various reasons. This includes calendar aging, which is degradation due to the passage of time, extreme temperatures, relatively large or low discharge, operating on the outer edges of the state of charge (SOC) and large depth of discharge (Vetter et al. 2005). An economic optimization should include battery degradation to represent the cost of battery usage. Furthermore, there are methods of mitigating the wear of the battery. One of these methods is avoiding the outer edges of SOC and keeping within an area where linear operation mechanics can be assumed. The size of the linear working area varies depending on the type of battery, but is centered around 50% state of charge (Laresgoiti et al. 2015). In this thesis, we assume that the linear working area is between 20-80% of SOC.

3.5 Control Hierarchy

Several layers of control are needed to achieve high-quality power in a micro-grid, each running at different sampling times. There are several ways to define the control layers, and in this thesis, the definition from Olivares et al. (2014) is used. The control hierarchy is shown in Figure 3.1.



Figure 3.1: General micro-grid control hierarchy.

Tertiary Control looks days or weeks into the future to find the optimal set-points for secondary control. Tertiary control is outside the scope of this thesis.

Secondary Control is the focus of this thesis. In the context of micro-grids, it is better known as the energy management system (EMS). The EMS schedules and controls the power balance, assuring that the power produced/imported matches the power demand. It is also responsible for future economic optimization and gives charging and discharging set-points for the ESS. An EMS will typically run several times every hour with fixed intervals and desirably calculate a solution in seconds. In this thesis, the EMS runs every 10 minutes.

Primary Control is mainly concerned with the power quality and balancing reactive and active power. Through methods like droop control, the primary controller stabilizes the voltage and the power frequency around the desired value and handles unforeseen disturbances in the power balance. It needs to act in a matter of milliseconds, as any large deviations in frequency can damage electrical components connected to the grid. In a traditional centralized grid, the primary controller relies on the system's inertia in the first few seconds after a power imbalance occurs. Synchronous generators, which are the backbone of the power industry, spin with the same frequency as the power frequency in the grid. Due to the inertia of all the synchronous generators, it takes a few seconds extra for a power imbalance to increase/decrease the frequency. This inertia is essential since it gives the primary controller 15-30 seconds to activate its frequency containment reserves, which are generators with a reserved capacity for production change in case of imbalances in the grid (ENTSOE 2019). While this effort might be enough, more significant imbalances need secondary and tertiary reserves. If the imbalance lasts several minutes, the secondary controller sets a new set-point for the production. There will often be a large fraction of the power produced by renewable energy sources that do not have synchronous generators or inertia in a micro-grid. This creates an extra challenge for the primary controller in micro-grids. Several proposals have been made, e.g. by Sandelic et al. (2018), Engels et al. (2020), where the energy storage system (ESS) acts like a primary controller. The lack of inertia in the power production can be mended by including quick response storage that can be activated in the matter of seconds, like spinning flywheels or ultra-capacitors. However, power quality and primary control is outside the scope of this thesis and will therefore not be discussed any further.

Chapter 4

Time Series Analysis and Forecasting

For the energy management system of the micro-grid to make economic decisions, it needs precise knowledge about the future. In this chapter, common methods used to describe and forecast *time series* are discussed.

A time series (TS) is a set of values obtained at successive points in time. A TS is called deterministic if future values are determined by a mathematical function $y = f(x, t)$. However, if the time-series future values can only be described by a probability function, the TS is called *statistical time-series* (Box & Jenkins 1990). As discussed in Chapter 2, PV production and load demands are intermittent signals and are in this thesis considered statistical time series.

Some essential definitions in the context of time series is needed for this chapter.

- *Stationarity* - A time-series is said to be stationary if the probability density function that describes the time-series is invariant under translation of time (Brown & Hwang 2012).
- *Trend* - The general direction of the data values over a period larger than the sampling time. For example: The stock market moving upwards over a 10 year period.
- *Seasonality* - Characteristic behaviour repeating itself in a periodic manner. For example: the sun rising every morning and setting every night.
- *Noise* - Random and unpredictable behaviour.

4.1 Evaluation of Time Series Forecasts

This section is based on the work done in the project thesis Husefest (2020).

Some metrics are defined to evaluate a time series forecast. A forecast \hat{y} looks N steps into the future, which is called the prediction horizon. \hat{y}_k is the prediction at step k in the prediction horizon. A prediction method is usually tested on a *test-set*, where the true signal y is known over the entire prediction horizon. The prediction error e at time k is defined as in Equation 4.1

$$e_k = y_k - \hat{y}_k \quad (4.1)$$

The metric used in this thesis is *root mean squared error* (RMSE), which is commonly used as forecast metrics, e.g. (Hans et al. 2018), (Labeeuw & Deconinck 2013). RMSE is defined as following

$$\text{RMSE} = \sqrt{\frac{1}{N} \sum_{k=1}^N (y_k - \hat{y}_k)^2} \quad (4.2)$$

An average over RMSE is used to evaluate the forecasting method over several time steps. The average RMSE, denoted A-RMSE, is

$$\text{A-RMSE} = \frac{1}{I} \sum_{i=0}^I \text{RMSE}_i, \quad (4.3)$$

where P is the number of forecasts, and RMSE_i is the RMSE over the entire prediction horizon at time-step i .

However, the nature of MPC, where only the first control action is chosen, suggests that the forecasts in the distant future are less important than those for the near future. Therefore, the one-step RMSE is defined as follows

$$1\text{-RMSE} = \sqrt{\frac{1}{I} \sum_{i=0}^I (y_{i,1} - \hat{y}_{i1})^2}, \quad (4.4)$$

where $y_{i,1}$ and $\hat{y}_{i,1}$ are the true values and the predicted values of the first prediction step respectively, and I is the simulation horizon.

As the system should be able to run on a real plant, computational time C is also important. C is defined as the average computational time per prediction,

$$C = \frac{1}{I} \sum_{i=0}^I C_i \quad (4.5)$$

So the three metrics A-RMSE, 1-RMSE, and computational time are used to evaluate the forecasting method. A-RMSE indicates how well the forecast catches the signal's general behavior, while 1-RMSE suggests how well the method performs in the near future.

4.2 Time Series Forecasting Methods

This section will be a short intro to different methods commonly used in time-series forecasting.

4.2.1 Feature-Driven Methods

A feature-driven method relies on external or exogenous time-series, for example, weather, season, etc. The major challenge that arises when using other exogenous TS for prediction is that these additional features also have to be predicted. Therefore the uncertainty from the feature prediction is propagated into the overall prediction method. Also, since the methods do not use any forecasting measurements, the 1-RMSE can be assumed to be high. However, several methods use this approach, for example, multiple linear regression, random forest, and *artificial neural network* (ANN), which was examined in Kayri et al. (2017).

Multiple linear regression (MLR) assumes a linear relationship $y_t = \mathbf{W}\mathbf{x}_t$ between the exogenous feature-vector \mathbf{x}_t , and the target time-series y_t . The weight-matrix \mathbf{W} is approximated by minimizing the least-square error $(y - \hat{y})^2$ in the training set. Predictions can then be computed by the matrix multiplication $\hat{y}_{t+1} = \mathbf{W}\hat{\mathbf{x}}_{t+1}$, where \hat{x} is a new set of exogenous values. The upside of using MLR is fast training and predictions, while the major drawback is the assumption of linear relationship between the features.

Random forest and ANNs are methods for learning nonlinear relationships $y = f(x)$, where y is the target time-series, x is the exogenous feature and $f(x)$ is an unknown function. It is outside the scope of this thesis to go into detail with these methods, despite showing high performance in, e.g., Kayri et al. (2017). The method demands a larger amount of data than what was available to this thesis. The authors in Kayri et al. (2017) had a year of data available, while we had less than two months. Furthermore, the increase in performance is low compared to the uncertainty in the exogenous features, as shown later in Chapter 6.3.

4.2.2 Stochastic Methods

This section is based on the work done in the project thesis Husefest (2020).

Stochastic methods are models that assume that the signal y is the output from white noise being fed through a linear filter (Moghran & Rahman 1989). There are two main models used in stochastic methods; auto-regressive (AR) and moving average (MA). AR models predict future values based on linear combinations of p previous values

$$y_t = c + \sum_{i=1}^p \phi_i y_{t-i} + w_t, \quad (4.6)$$

where c is a constant, ϕ are the parameters, and w_t is white noise. MA models uses past errors from q previous predictions to predict future values on the form

$$y_t = c + \sum_{i=1}^q \theta_i w_{t-i} \quad (4.7)$$

where w_t is white noise, and θ are the parameters.

AR and MA models can be combined into an ARMA model, where predictions are made from both Equation 4.6 and Equation 4.7. However, AR, MA, and ARMA require the TS to be stationary (Box & Jenkins 1990). A non-stationary signal can be transformed into a stationary signal by *differencing*. Differencing transforms the time-series $y(t)$ to the time-series $d(t)$ with the recursive formula

$$d^I(t) = d^{I-1}(t) - d^{I-1}(t-1),$$

where I is the number of times the TS is differenced and $d^0(t) = y(t)$. If this is needed, the ARMA model is extended to an ARIMA model. The added I stands for *integrated*, which is the number of times the signal has to be "un-differenced" to get the prediction y . If the time-series also has seasonal components, the ARIMA model can be extended to a seasonal ARIMA or SARIMA.

Moghram & Rahman (1989) shows that ARIMA gives high performance for predicting load demands on a short-term basis. Also, since they rely on the current measurement, the one-step predictions are usually good. However, the main drawbacks are complex models that require high computational power and difficulties handling noisy signals (Husefest 2020).

4.2.3 Knowledge-Based Methods

Knowledge-based methods are rule-based methods, which are built up from domain knowledge of the signal. These rules can be simple, for example, power demand on weekdays is larger than on weekends, or more complex rules and systems like in Labeeuw & Deconinck (2013). The authors analyze thousands of residential load profiles and clusters them together as groups of similar behavior within each quarter of a year. These methods are good at capturing the typical trends over a day and can be computed offline. However, they neglect measurements and therefore have lower accuracy for one-step predictions.

4.2.4 Mathematical Models

In some cases, it is possible to express the time-series function mathematically, for example, in photovoltaic cells. Although a perfect mathematical model will predict the time series without error, this is not possible in practice due to parameter uncertainties and modeling assumptions.

Symbol	Explanation	Type
I	Current	Output variable
V	Voltage	Output variable
G	Global horizon irradiance	Input variable
T	Temperature	Input variable
I_{PV}	Photovoltaic current	PV parameter
I_0	Saturation current of PV diode	PV parameter
I_{rs}	Reverse saturation current	PV parameter
I_{sc}	Short circuit current	PV parameter
V_{OC}	Open circuit voltage	PV parameter
N_s	Number of PV-cells connected in series	PV parameter
A	Diode ideality factor	PV parameter
R_s	Series resistance	PV parameter
R_p	Parallel resistance	PV parameter
E_g	Energy band gap	PV parameter
K_i	Model constant	PV parameter
T_{nom}	Reference temperature	PV parameter
G_{nom}	Reference global horizon irradiance	PV parameter
q	Electron charge	Physical constant
K	Boltzmann constant	Physical constant

Table 4.1: Parameter for PV model optimization problem.

PV model An initial PV model was developed with the help of SINTEF, was based on Vinod et al. (2018), Junior (2016) and Villalva et al. (2009). This model was based around an optimization problem that used air temperature and irradiance to calculate the power.

$$I_{PV} = \frac{G}{G_{nom}}(I_{sc} + Ki(T - T_{nom}))$$

$$I_0 = I_{rs} \left(\frac{T}{T_{nom}} \right)^3 e^{\frac{qE_g}{AK}} (1/T_{nom} - 1/T) \quad (4.8)$$

$$I_{rs} = I_{sc} e^{-\frac{qV_{oc}}{N_s K A T}}$$

$$I = I_{pv} - I_0 * e^{\frac{V + R_s I}{V_t a} - 1} - \frac{V + R_s I}{R_p} \quad (4.9)$$

The model created an optimization problem, with voltage and current as decision variables, which should satisfy Equation 4.9, and the sub equations in 4.8. The predicted power production was then calculated by multiplying the voltage V and current I .

As discussed later in Chapter 6.3, the model provided accurate predictions. However, the main drawbacks of the method is the computational time needed to solve the optimization problem and the uncertainty in the parameters.

Model Predictive Control

In the literature study (Chapter 2.4), model predictive control (MPC) is proposed as a control scheme in the energy management system of a micro-grid. However, there are variations of MPC, and the most relevant in this thesis is the economic MPC (EMPC).

This chapter starts by going through dynamic optimization and optimal control problems, which leads to the introduction of MPC. Then an elaboration on the challenges and advantages of using an EMPC compared to a nominal MPC scheme is presented. Furthermore, robust and stochastic versions of MPC are discussed, which leads to the scenario-tree MPC. The chapter ends with a description of direct shooting methods used to solve optimization problems numerically.

5.1 Dynamic Optimization and Optimal Control Problems

Optimization problems are also known as mathematical programming problems, and the task is to find the best values given some criteria. Since most programming problems cannot be solved explicitly, it is common to use numerical methods, which is discussed in Chapter 5.5. Comprehensive literature exists on the topic, e.g. *Numerical Optimization* by Nocedal & Wright (2006).

A constrained optimization problem can be written as in Equation 5.1, where $L(x)$ is a function to be minimized, and x is the decision variable. $c_i(x)$ are the constraints, with \mathcal{E} being the index set for the equality constraints and \mathcal{I} being the index set for the inequality constraints. $L(x)$ is often called *objective* or *cost function*. The set of values defined by the constraints is called the feasible region and includes the optimal solution. Note that a maximization problem can easily be manipulated into the standard form of a minimization problem by changing the sign of $L(x)$.

$$\begin{aligned}
& \min_x && L(x) \\
& \text{s.t.} && c_i(x) = 0, \quad i \in \mathcal{E} \\
& && c_i(x) \geq 0, \quad i \in \mathcal{I}
\end{aligned} \tag{5.1}$$

An fundamental concept of optimization is *convexity*, which can be used for both sets and functions. The definitions are collected from Nocedal & Wright (2006).

- A set $S \in \mathbb{R}^n$ is *convex* if a straight line segment connecting any two points in S lies entirely inside S .
- A function f is *convex* if its domain S is a convex set, and for any two points x and y , the following property is satisfied.

$$f(\alpha x + (1 - \alpha)y) \leq \alpha f(x) + (1 - \alpha)f(y) \quad \alpha \in [0, 1] \tag{5.2}$$

If $-f$ is *convex*, f is said to be *concave*.

Convexity is useful due to the following statement; if the objective function L in Equation 5.1 and the feasible region are both convex, then any local solution is a global solution (Gros & Diehl 2017).

A special case of constrained optimization is linear programming (LP) where the function $L(x)$ and all the constraints $c(x) \in \{\mathcal{E}, \mathcal{I}\}$ are linear. LP is well researched and can be solved efficiently with method such as *simplex* or *interior-point* methods (Nocedal & Wright 2006).

Nonlinear Programming (NLP) problems are more common and occur when either $L(x)$ or any of the constraints are nonlinear functions. A special case of NLPs are quadratic programming (QP) problems. QPs are characterized by a quadratic objective function and linear constraints. If the objective function is convex, *active-set* or *interior-point* methods can efficiently solve QP problems.

Other types of optimization include integer programming (IP), where the variables can only take integer values, and mixed-integer programming (MIP), where only some of the variables must have integer values.

5.1.1 Optimal Control

Optimal control is an optimization method used to derive control policies for systems on the form

$$\begin{aligned}
\dot{x} &= f(x, u) \\
y &= g(x),
\end{aligned} \tag{5.3}$$

where x are the states of the system, u are the controllable input to the plant, $f(x, u)$ is a function that describes the system's dynamics, and y is the observable output of the plant.

In optimal control, the control policy or trajectory of (x, u) is the sequence of solutions to the *optimal control problem* (OCP). Equation 5.4 shows a continuous OCP, from $t = 0$ to $t = T$. Equation 5.4a is the objective function, ℓ is called the stage-cost and $V(x_N)$ is a cost on the terminal state. The dynamics of the system is included as a constraint (Equation 5.4b), which together with path constraints (Equation 5.4c), and terminal constraint (Equation 5.4d) make up the feasible region of the problem.

Many control problems are open-ended and has infinite horizon, such as in a micro-grid operation. Therefore, the prediction horizon N should also be infinite. However, this is generally not numerically possible to compute. Therefore, the terminal cost $V(x_N)$ is included to approximate an infinite horizon. This will be discussed further in Chapter 5.3.3.

$$\min_{x,u} \int_0^T \ell(x(t), u(t)) dt + V(x(T)) \quad (5.4a)$$

$$s.t. \quad \dot{x} = f(x(t), u(t)) \quad (5.4b)$$

$$0 \geq h(x(t), u(t)) \quad (5.4c)$$

$$x(T) \in \mathcal{T} \quad (5.4d)$$

5.2 Model Predictive Control

Although optimal control can find control policies for dynamic systems, the plant may behave differently than expected. This behavior is due to differences between the real plant and the mathematical model used in the optimization, often called *model-plant-mismatch* (Gros & Diehl 2017). The approach described in the previous section is *open-loop control*, as calculations are done offline, without updates from the plant. Model Predictive Control (MPC), however, is a *closed-loop control* scheme that incorporates *feedback* from the plant. At every time step, the MPC recalculates an OCP based on measurements collected from the plant. The general MPC algorithm is shown in Algorithm 1.

Algorithm 1 General MPC Algorithm

for $k = 0, 1, 2, \dots$: **do**

1. Get the current state x_k
2. Solve a constrained optimization problem on the horizon from k to $k+N$.
3. Apply first control move u_k from the solution above

end for

The objective of a standard MPC is generally to stabilize the states to a given set-point or trajectory (Angeli et al. 2012). Therefore, the cost function should be designed such that the optimal state and associated control (x^*, u^*) gives zero cost.

$$0 = \ell(x^*, u^*) \leq \ell(x, u) \quad x \in \mathcal{X}, u \in \mathcal{U} \quad (5.5)$$

Mayne et al. (2000) offers stability proofs on several MPC schemes, under the assumption of Equation 5.5 and enforcing some additional assumptions on the terminal constraints and costs. Details about these additional assumptions are not included in this thesis, but recommended literature can be found in Mayne et al. (2000) and Faulwasser et al. (2018).

5.3 Economic Model Predictive Control

When dealing with the optimization of economic processes, the traditional method has been to decompose the problem into two stages (Angeli et al. 2012). The first stage is often called real-time optimization (RTO) and finds optimal steady-state references. The second stage uses, for example, MPC as described in the previous section to track the references. The RTO usually recalculates the references on an hours-to-day basis, while the MPC updates on the rate of seconds to minutes (Ellis et al. 2014). This method is denoted *tracking MPC* from this point.

However, an economic MPC (EMPC) removes the steady-state optimization and minimizes the economic cost directly. Besides removing the RTO, EMPC has benefits such as allowing for time-varying systems and transient economic control. Transient economic control means that the EMPC can reach the optimal value and find the most economical way to get there. This principle is illustrated next with an example by Rawlings & Amrit (2009), which compares an EMPC and a tracking MPC.

5.3.1 Example: Tracking vs. Economic MPC

Let us consider the following linear system with the discrete dynamics

$$x_{k+1} = \begin{bmatrix} 0.857 & 0.0883 \\ -0.0147 & -0.0151 \end{bmatrix} x_k + \begin{bmatrix} 8.57 \\ 0.884 \end{bmatrix} u, \quad (5.6)$$

where $x \in \mathbb{R}^2$, $u \in \mathbb{R}$, and inputs constrains $u \in [-1, 1]$. The economics which should be minimized are defined as

$$\ell_{eco}(x, u) = -[3, 2]^T x - 2u \quad (5.7)$$

Due to the constraint $u \in [-1, 1]$ and the linear economics, the optimal input is $u^* = 1$, which corresponds to the states $x^* = (60, 0)$. The cost-function for the tracking MPC is defined as

$$\ell_{targ}(x, u) = [(x_1 - x_1^*)^2 + (x_2 - x_2^*)^2 + (u - u^*)^2] \quad (5.8)$$

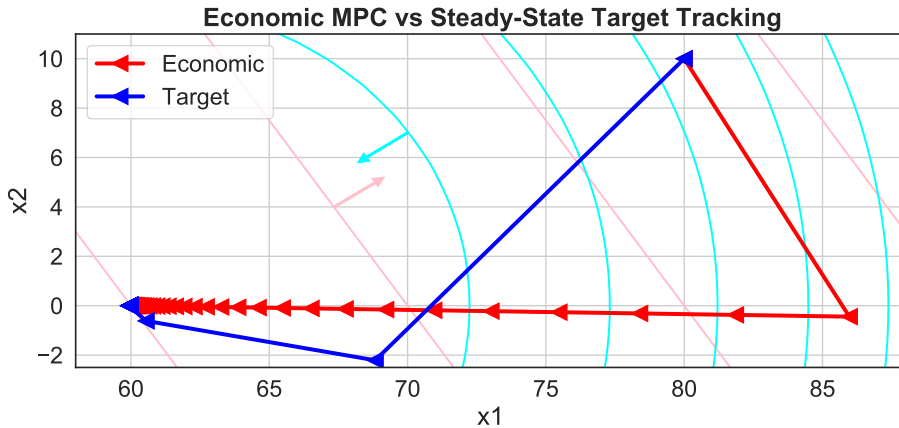


Figure 5.1: Economic MPC and tracking MPC. The pink vector shows the increasing costs, while the cyan vector shows decreasing set-point error.

Figure 5.1 shows the trajectory of the two MPC schemes, both initialized at $x = (80, 10)$. The EMPC earned 7943 units, which is a 6% increase of the tracking MPC's profit of 7472 units. The EMPC takes a slow path to reach the optimal set-point while tracking MPC is inconsiderate of the economics and rushes to the same point fast.

5.3.2 EMPC Stability

Unlike the cost-function in Equation 5.5, the EMPC stage cost is not necessarily positive. Consequently, classical stability proofs fail (Faulwasser et al. 2018). Therefore energy-based stability proofs have been researched for EMPC, and Diehl et al. (2011) shows that the system is stable if the problem is *dissipative*. An intuitive definition of dissipative system is; *the rate of increase in energy is no greater than the input power* (Bao & Lee 2007).

To prove dissipativity, one has to find a storage function that satisfies the dissipativity inequality (Faulwasser et al. 2018), which is non-trivial. It is outside the scope of this thesis to examine this further, but several methods have been proposed to find this storage function in recent literature. Pirkelmann et al. (2019) proposes to use a sum-of-squares method, Scherer & Weiland (2020) uses linear matrix inequalities and Koch et al. (2020) uses noisy data from linear systems.

5.3.3 Dynamic Programming and Terminal Costs

Another issue with the non-tracking behavior of EMPC occurs if the prediction horizon N is short compared to the system dynamics and a terminal cost is not used. An OCP has a limited prediction horizon, and ideally, the OCP of the

micro-grid EMPC should have an infinite prediction horizon. Still, it is not computationally feasible to include all time steps in our OCP. The time steps after the horizon are still a part of our problem, and a short prediction horizon can create some unwanted effects. An example from using EMPC on micro-grids can illustrate these effects, which is demonstrated in Chapter 7.1. With a short horizon, the controller with a short prediction horizon depletes the battery to earn money. However, with a long prediction horizon, the EMPC keeps more energy in the battery, which is more economical in the long run.

Terminal cost is a term or function $V(x_N)$ in the objective function representing the cost of terminating the optimization horizon at different state values. Ideally, this term should penalize end states that would be disadvantageous as an initial value for the OCP. One method for finding the terminal cost expression is *dynamic programming*.

Dynamic programming is based on the concept that any sub-sequence of an optimal sequence is the optimal solution to the sub-problem and vice versa. By using this principle, complex problems can be divided into sub-problems and solved separately before re-assembling the solutions. As applied here for terminal cost calculation, the method finds the optimal action given the state of charge by calculating the cost for the optimal action. The Bellman function, also known as the value function, is the expression used in dynamic programming. It consists of a stage cost and a next step cost term.

$$V(x) = l(x, u) + \gamma V(x_+), \quad (5.9)$$

where x_+ is the next value of the state.

The value function iteration method can be used to find the solution of equation 5.9. This method iterates over the function and is shown in Algorithm 2. At each iteration, all possible value combinations of u and x are calculated and stored. The algorithm then chooses the smallest value for each state and continues the iteration until some predefined error bound is reached. The coefficient γ is the discount factor, enforcing convergence for values between $[0,1)$.

Algorithm 2 Value Iteration Method

Require: $V = 0$
while $Error > \epsilon$ **do**
 for all states **do**
 for all inputs **do**
 $Q(x, u) \leftarrow l(x, u) + \gamma V(x_{next})$
 end for
 $V(x) \leftarrow \min_u Q(x, u)$
 end for
 $Error \leftarrow V - V_{prev}$
 $V_{prev} \leftarrow V$
end while

5.4 Scenario-Tree MPC

As mentioned in Chapter 5.2, model-plant-mismatch can happen in the modelling, either via parameter uncertainty, or via exogenous disturbance $w(t)$. In this thesis it is assumed that the parameter uncertainty is negligible, which means the dynamic system in Equation 5.3 can be extended to

$$\dot{x} = f(x, u, w) \tag{5.10}$$

Some of the uncertainties can be mitigated by an MPC scheme due to the closed-loop control. However, the uncertainties affect performance, and if they are large, they can push the system outside the constraints and give an infeasible solution. This problem has led to robust and stochastic MPC development, which incorporates uncertainties into the MPC formulation. In this thesis, scenario-tree MPC is implemented due to the nature of the disturbances in the system. This is discussed next in the context of robust and stochastic MPC.

5.4.1 Robust and Stochastic MPC

The difference between robust and stochastic MPC lies in the knowledge about the uncertainty $w(t) \in \mathbb{R}^p$ (Mayne 2016). Robust MPC assumes $w(t)$ is contained within a closed set $\mathbb{W} \in \mathbb{R}^p$. This assumption means that the uncertainty is bounded, and MPC can ideally find solutions that satisfy the constraints. Raković (2019) offers literature on several implementations of robust MPC. The main drawbacks of the methods are concerning the assumption of bounded uncertainties. A large set \mathbb{W} can lead to conservative behavior and bad performance, and even infeasible problems.

On the other hand, in stochastic MPC, $w(t)$ is described as a random process with probability distribution ϕ , which is generally assumed to be unbounded. This means that one can no longer guarantee constraint satisfaction, which is solved by using chance- or expectation constraints (Heirung et al. 2018). Chance constraints are designed such that the probability of violating constraints is kept under a given threshold, while expectation constraints force the MPC to satisfy the constraints in expectation. Another challenge in stochastic MPC is to represent ϕ in a finite and computationally tractable way (Mayne 2016).

Scenario-tree MPC can be used to implement both robust and stochastic MPC, depending on how the scenarios represent the uncertainty. If the disturbance is assumed bounded, the scenarios can span out the most extreme realizations, resulting in a robust MPC (Raković 2019). Scenario-tree are also used in stochastic MPC, for example, in Hans et al. (2018), where the authors used Monte-Carlo simulations to represent the probability distribution. However, accurately representing the uncertainty via this method requires a large number of simulations. Furthermore, *scenario-reduction* (Heitsch & Römich 2003) is used to find a tractable number of scenarios. Consequently, this method is criticized by Mayne (2016) due to the high

computational complexity.

A scenario-tree MPC can roughly be split into two parts; creating a scenario tree that spans different discrete realizations of the uncertainty in the prediction horizon and solving the OCP that minimizes the expected objective function over all scenarios.

5.4.2 Scenario Tree

At each time-step, the MPC optimizes over a scenario tree as shown in Figure 5.2. For each step in the prediction horizon, the tree splits into b branches, where b is called the *branching factor*. This leads to an exponential growth in number of scenarios S , more precisely $S = b^N$. In order to reduce the complexity of the optimization problem, a robust horizon N_r is defined. As shown in Figure 5.2, the tree will create new branches up to N_r , yielding $S = b^{N_r}$. If $N_r = 0$, the problem reduces to a nominal MPC. $N_r = 2$ is called a *two-stage* MPC, while $N_r > 2$ is called a *multi-stage* MPC.

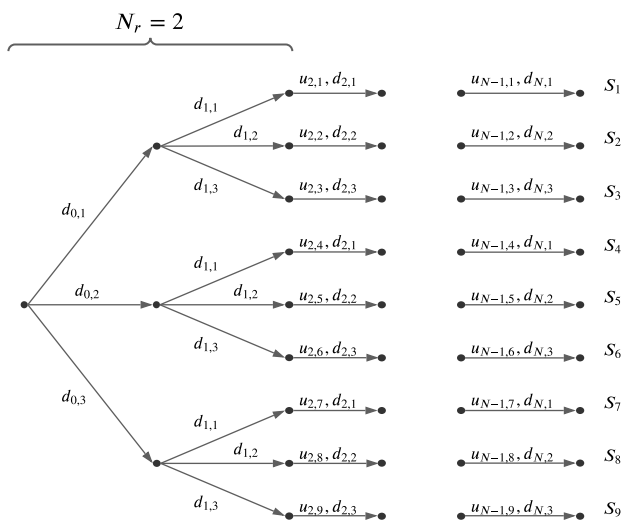


Figure 5.2: Scenario Tree with $b = 3$, and $N_r = 2$

5.4.3 Optimization Problem

A discrete scenario-tree optimization problem can be written as in Equation 5.11 (Krishnamoorthy, Foss & Skogestad 2018). w_j is a weight associated with the respective scenario and usually reflects the probability of the realization.

$$\min_{\mathbf{x}_j, \mathbf{u}_j} \sum_{j=1}^S \left[w_j \sum_{k=0}^N J(x_{j,k}, u_{j,k}) \right] \quad s.t. \quad (5.11a)$$

$$x_{j,k+1} = f(x_{j,k}, u_{j,k}, d_{j,k}) \quad (5.11b)$$

$$g(x_{j,k}, u_{j,k}) \leq 0 \quad (5.11c)$$

$$\sum_{j=1}^S \bar{\mathbf{E}}_j \mathbf{u}_j = 0 \quad (5.11d)$$

The last constraint Equation 5.11d is a non-anticipativity constraint which couples the scenarios together in the tree structure. Since a node cannot anticipate a future disturbance, all children from a node needs to have the same control input. \mathbf{u}_j is the vector containing control inputs for a single scenario j , i.e. $\mathbf{u}_j = [u_{0,j}, u_{1,j}, \dots, u_{N-1,j}]$. To define the matrices $\bar{\mathbf{E}}_j$, Klintberg & Gros (2017) introduces the notation:

$$p = n_u \sum_{j=1}^{S-1} n_{c,(j,j+1)} \quad (5.12)$$

where $n_{c,(j,j+1)}$ is the number of common nodes in between two consecutive scenarios. $\bar{\mathbf{E}}_j \in \mathbb{R}^{p \times n_u N}$

$$\bar{\mathbf{E}} = \left[\begin{array}{c|c|c|c|c} E_{1,2} & -E_{1,2} & & & \\ & E_{2,3} & -E_{2,3} & & \\ & & \ddots & & \\ & & & \ddots & \\ & & & & E_{S-1,S} & -E_{S-1,S} \end{array} \right] \quad (5.13)$$

$$\bar{\mathbf{E}} = [\bar{\mathbf{E}}_1 \mid \bar{\mathbf{E}}_2 \mid \dots \mid \bar{\mathbf{E}}_S]$$

and

$$E_{j,j+1} = \left[\begin{array}{c|c} I_{n_u} & \\ & \ddots \\ & & I_{n_u} \end{array} \middle| \mathbf{0} \right] \in \mathbb{R}^{n_u n_{c,(j,j+1)} \times n_u N} \quad (5.14)$$

5.4.4 Approximated Scenario MPC

Due to the nature of MPC, where only the first control input is used, the uncertainties in the near future will affect the system more than in the distant future. A simpler scenario-tree MPC can therefore be formulated to reduce computational time.

The non-anticipativity constraint are relaxed, and only the inputs in the root node $u_{0,j}$ are forced to be equal (Klintberg et al. 2016). This gives us the optimization problem in Equation 5.15, where only Equation 5.15d is different from Equation 5.11.

$$\min_{\mathbf{x}_j, \mathbf{u}_j} \sum_{j=1}^S \left[w_j \sum_{k=0}^N J(x_{j,k}, u_{j,k}) \right] \quad s.t. \quad (5.15a)$$

$$x_{j,k+1} = f(x_{j,k}, u_{j,k}, d_{j,k}) \quad (5.15b)$$

$$g(x_{j,k}, u_{j,k}) \leq 0 \quad (5.15c)$$

$$u_{j,0} = u_{l,0}, \quad j, l \in [0, 1, \dots, S], j \neq l \quad (5.15d)$$

5.5 Numerical Optimization

Numerical methods are necessary to solve continuous OCP as in Equation 5.4. Although several methods exist, this section will focus on direct methods. A direct method aims to parameterize a continuous OCP, which has infinite decision variables, into a finite-dimensional nonlinear program (Gros & Diehl 2017). In practice, this translates to "first discretize, then optimize". There are three important classes of direct methods; *direct single shooting*, *direct multiple shooting* and *direct collocation*. However, since shooting methods are used in this thesis, direct collocation is not discussed further.

5.5.1 Direct Single Shooting

Single shooting, e.g. (Hicks & Ray 1971), starts by parametrizing the control inputs $u(t)$ into polynomials, where piecewise constant controls are most often used (Gros & Diehl 2017). The discrete input parameters are called q , giving the resulting control function $u(t, q)$. The time horizon T is divided into N intervals, where $0 = t_0 < t_1 \dots < t_N = T$. The discrete input parameter can then be denoted $q_k = u(t, q)$. By using an ordinary differential equation (ODE) solver, the dynamics of the system (Equation 5.4b) substituted into the the cost and path constraints of the OCP. This gives the NLP shown in Equation 5.16. Since the problem is only dependent on q , it can be solved by NLP methods such as Sequential Quadratic Programming (SQP) or IPOPT (Chapter A.1), and integrating forward from the initial value $x(0)$.

$$\min_q \int_0^T \ell(x(t, q), u(t, q)) dt + \Psi(x(T, q)) \quad (5.16a)$$

$$s.t. \quad 0 \geq h(x(t, q), u(t, q)) \quad (5.16b)$$

$$x(T, q) \in \mathcal{T} \quad (5.16c)$$

5.5.2 Direct Multiple Shooting

Direct multiple shooting uses the same constant input parametrization of $u(t)$ as single shooting, $u(t) = q_i$, $t \in [t_i, t_{i+1}]$. However, unlike single shooting, each interval solved the ODE separately with the arbitrary initial values s_i .

$$\dot{x}_i(t, s_i, q_i) = f(x_i(t, s_i, q_i), t \in [t_i, t_{i+1}]) \quad (5.17)$$

$$x_i(t, s_i, q_i) = s_i \quad (5.18)$$

Furthermore is the cost-function integrated in equation 5.19

$$\ell_i(s_i, q_i) := \int_{t_i}^{t_{i+1}} L(x_i(t_i), s_i, q_i) dt \quad (5.19)$$

This results in the discrete OCP

$$\min_{s, q} \sum_{k=0}^{N-1} \ell(s_k, q_k) + \Psi(s_N) \quad (5.20a)$$

$$s.t. \quad 0 = x_0 - s_0 \quad (5.20b)$$

$$0 = x_i(t_{i+1}, s_i, q_i) - s_{i+1} \quad (5.20c)$$

$$0 \geq h(s_i, q_i) \quad (5.20d)$$

$$s_N \in \mathcal{T}, \quad (5.20e)$$

where Equation 5.20b is for initial value, Equation 5.20d are the path constraints and Equation 5.20e is the terminal constraint. Since each interval is solved individually, Equation 5.20c is required to ensure continuity over the trajectory.

Chapter 6

Methodology

This chapter presents the methods used to address the research questions in Chapter 1. A mathematical model of the Skagerak EnergyLab is developed and presented as an optimal control problem. Next, a time series analysis of solar production and load demands is discussed, culminating in the prediction methods used in the results. Next, the mathematical model is extended to incorporate the uncertainties from the prediction methods in the form of a scenario-tree MPC. Finally, the uncertainties are analyzed, and the methods for selecting scenarios are presented.

Figure 6.1 shows the overall architecture of the system. The sections of this chapter detail each component of the system, while the next paragraph gives a brief overview of the system.

At every time step, the system starts by collecting measurements and numerical weather predictions from the external source. Predictions of PV production and load demands are then calculated and fed into the energy management system (EMS), together with the current state of charge (SOC). The EMS is where the developed MPC scheme runs on a 10 minute sampling time and calculates optimal setpoints for the battery and grid. If the EMS fails to balance the powers after the real PV production and load, the error is fixed by a primary controller. This is done by buying extra or selling surplus energy to the grid. The new state of charge of the battery is then simulated based on the battery inputs.

6.1 Mathematical Modeling

The mathematical formulation for an economic model predictive control (EMPC) scheme should reflect the real-life economics of micro-grid. As discussed in Chapter 2.3.2, the current economics are dependent on a consumption-based fixed grid tariff, denoted q_{fixed} . However, this will most likely change to an effect-based tariff NVE (2018), denoted here as q_{peak} .

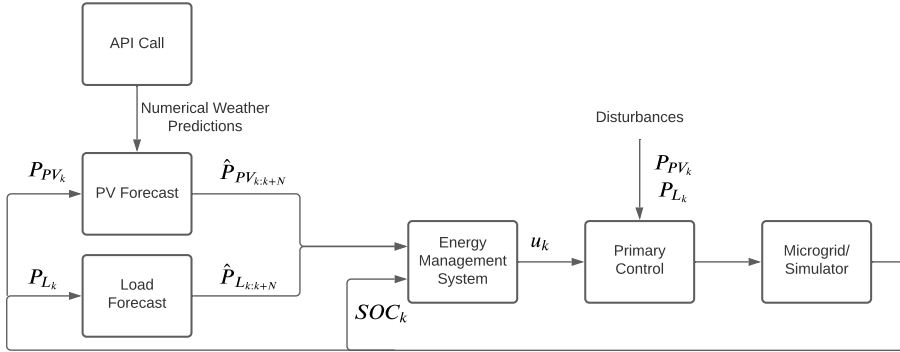


Figure 6.1: System Architecture.

6.1.1 Topology

Skagerak Energylab consists of a battery energy storage system, an array of photovoltaic (PV) cells, and loads. Figure 1.1 shows the original topology of the system. However, the system can be configured as to virtually be represented as in Figure 6.2.

From Kirchhoff's junction law, the sum of all currents, I , should be zero in a node. Furthermore $P = VI$ and the voltage is kept constant at $V = 0.4\text{kV}$. Therefore, the sum of all powers should also be zero. This leads to the topology constraint

$$P_G + P_{PV} - P_B - P_L = 0, \quad (6.1)$$

where P_G , P_B are the powers exchanged with the grid and battery respectively. P_{PV} is the power delivered from the photovoltaic cells and P_L are the load demands. P_G is defined such that positive values refer to buying energy, and consequently negative values means selling. Furthermore, P_B is defined such that positive values refer to charging, and negative values means discharging the battery.

6.1.2 Inputs

The inputs P_G and P_B are split into two positive signals, defined in Equation 6.2 and Equation 6.3 (Husefest 2020). For the grid signals, P_G , the separation is done as a lower price is assumed when selling compared to buying. The main reason the battery signals are split is due to the degradation model, which is proportional to the absolute charge/discharge of the battery. Newton-based solvers, for example, IPOPT Chapter A.1, which is used in this thesis, require the cost function to be differentiable. Therefore the absolute value cannot be used directly. Splitting the signal into two positive signals avoids using the absolute value function. Another reason for splitting the signals is that the battery coefficient can vary for charging and discharging.

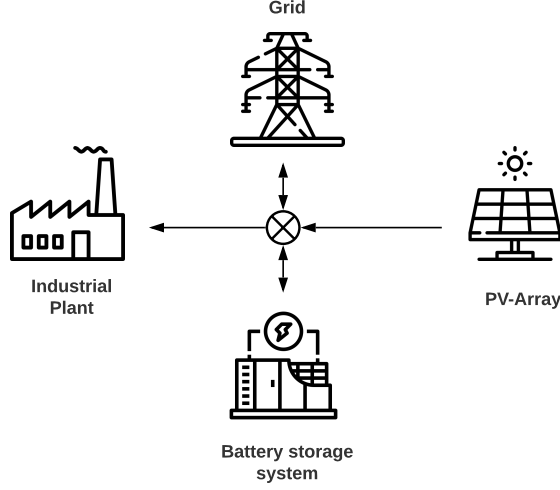


Figure 6.2: Simplified topology of Skagerak Energylab.

The constraints Equation 6.2b and Equation 6.2c are to ensure that one cannot exceed the maximum capacity of the grid $P_{G,max}$. Equation 6.3c and Equation 6.3d are to ensure the maximum charge and discharge power of the battery is not exceeded.

$$P_G = P_{G_b} - P_{G_s} \quad (6.2a)$$

$$0 \leq P_{G_b} \leq P_{G,max} \quad (6.2b)$$

$$0 \leq P_{G_s} \leq P_{G,max} \quad (6.2c)$$

$$P_B = P_{B_c} - P_{B_d} \quad (6.3a)$$

$$|P_B| = P_{B_c} + P_{B_d} \quad (6.3b)$$

$$0 \leq P_{B_c} \leq P_{B,max} \quad (6.3c)$$

$$0 \leq P_{B_d} \leq P_{B,max} \quad (6.3d)$$

To simplify notation going further the input-vector u is defined as

$$u = [P_{B_c}, P_{B_d}, P_{G_b}, P_{G_s}]^T$$

6.1.3 States and Differential Equation

The first state in the system is the battery state of charge (SOC), which is a percentage of the maximum capacity C_{max} . Mathematically the battery works as

a pure integrator, as it only depends on the power accumulated and dissipated. The resulting continuous differential equation is

$$\dot{x} = \frac{\eta_c P_{B_c}}{C_{max}} - \frac{P_{B_d}}{\eta_d C_{max}}, \quad (6.4)$$

where η_c and η_d are the charge and discharge coefficient respectively. The battery coefficients $\eta_i \in [0, 1]$ $i \in \{c, d\}$ reflects the efficiency of the battery, and that some energy is lost during charging and discharging. Recall from Equation 6.3 that P_{B_c} and P_{B_d} are non-negative. Therefore the first term charges the battery in Equation 6.4, giving an increase in SOC, while the second term discharges the battery.

The second system state is the grid peak power G_P , which is the maximum power drawn from the grid. The controller should minimize the peak due to the effect-based tariff discussed in Chapter 2.3.2. The state evolution $G_{P,k+1}$ is defined as the maximum of the power bought from grid P_{G_b} and the peak power at the previous time-step as in Equation 6.5

$$G_{P,k+1} = \max \left\{ \begin{array}{l} G_{P,k} \\ P_{G_b,k} \end{array} \right\} \quad (6.5)$$

However, since max is a non-differentiable operator, it cannot be used directly in the solver. In implementation, Equation 6.5 is therefore transformed to two inequality constraints as in Equation 6.6. Since $G_{P,k+1}$ is minimized in the cost function, $G_{P,k+1}$ will always be equal to one, and not greater than both of $P_{G_b,k}$ and $G_{P,k}$.

$$\begin{aligned} G_{P,k+1} &\geq G_{P,k} \\ G_{P,k+1} &\geq P_{G_b,k} \end{aligned} \quad (6.6)$$

To simplify notation going further the state-vector x is defined as

$$x = [SOC, G_P]^T$$

6.1.4 Stage Costs

The cost function in an EMPC should reflect the economics of the system directly. This section is therefore based on the discussions in Chapter 2.3.

The first term in the state-cost is related to the battery degradation, which is assumed equal and linear for charging and discharging, and proportional with a degradation coefficient C_{deg} . The battery stage-cost is therefore defined as in Equation 6.7, where the second step follows from Equation 6.3.

$$\begin{aligned} \ell_B(u_k) &= C_{deg} |P_{B,k}| \\ &= C_{deg} (P_{B_c,k} + P_{B_d,k}) \end{aligned} \quad (6.7)$$

The grid costs include two terms. The first term is the exchange with the grid, where the costs are defined by the spot-price E . The TSO usually requires a fee

for energy sold to the grid (Berg et al. 2021), which is dependent on the amount of energy sold. It is here simplified by assuming a 10% tax for selling electricity.

The other cost is the grid tariff. Both the current consumption-based fee and the future effect-based fee is modeled. The fixed fee is a fixed price per kWh bought from the grid q_{fixed} , and we assume there is no tariff when selling to the grid. This gives the stage-cost

$$\ell_{G_f}(u_k) = E_k(P_{G_b,k} - 0.9P_{G_s,k}) + q_{fixed}P_{G_b,k}, \quad (6.8)$$

where the term $0.9P_{G_s,k}$ reflects the 10% tax discussed earlier.

The new price model is the effect-based tariff, where the peak G_P should be kept as low as possible. In practice, this cost is billed once a month and should therefore be modeled as a terminal cost $q_{peak}G_P$, where q_{peak} is the effect fee. However, this is unpractical in an MPC that operates with a prediction horizon that is hours-to-day. Therefore the terminal cost is transformed into a stage cost $q_{peak}(G_{P,k+1} - G_{P,k})$. This gives the grid stage-cost

$$\ell_{G_p}(u, k) = E_k(P_{G_b,k} - 0.9P_{G_s,k}) + q_{peak}(G_{P,k+1} - G_{P,k}) \quad (6.9)$$

This gives two expressions for the stage-costs, summarized in Equation 6.10.

$$L_m(u) = \sum_{k=0}^{N-1} \ell_B(u_k) + \ell_{G_m}(u_k) \quad m \in \{p, f\} \quad (6.10)$$

6.1.5 Terminal Cost

The terminal cost was found by using dynamic programming and the Bellman equation as discussed in 5.3.3. The Bellman equation implementation for calculating the terminal cost was 6.11.

$$V(x) = \min_{P_G, P_B} EP_G + C_{deg}P_B + S_x + \gamma V(x_+), \quad (6.11)$$

where E is spot-price, C_{deg} is the degradation coefficient, P_G and P_B are the powers exchanged with grid and battery. S_x is penalty on values outside the allowed range.

The solution was found using the value iteration method (Algorithm 2). Before the algorithm was used, the states and the inputs were discretized. The state x is a set of discrete SOC values in the range $[0,1]$ and the inputs of the system is a set of discrete grid values, P_G , from $[-1000, 1000]$. The battery P_B was determined by the Equation 6.1, where the load and PV were given by their expected values. The next value of of the state, x_+ is determined by the battery, according to Equation 6.4. If x_+ is outside $[0,1]$, then S_x is an infinitely large value and if it is not outside its bound, S_x is 0. This term penalizes the constraint violations of the state of charge. The result of the algorithm is an array of values with corresponding states, x . The array was interpolated to find a linear function $V(x)$ (Equation 6.12), that was used as the terminal cost function in the OCP.

$$V(x) = ax + b \quad (6.12)$$

6.1.6 Optimal Control Problem

The micro-grid optimal control problem stated in Equation 6.13 summarizes the Equation 6.1 - Equation 6.11. The economic cost function makes the resulting MPC-scheme an EMPC. Since there is no uncertainty handling in the EMPC, it is called deterministic EMPC (DEMPC).

$$\begin{aligned}
& \min_{x,u} \sum_{k=0}^{N-1} \ell_B(u_k) + \ell_{G_m}(u_k) + V(x_N) \quad , m \in \{p, f\} \\
& \quad s.t. \\
& SOC_{k+1} = \frac{\eta_c P_{B_c,k}}{C_{max}} - \frac{P_{B_d,k}}{\eta_d C_{max}} \\
& G_{P,k+1} \geq G_{P,k} \\
& G_{P,k+1} \geq P_{G_b,k} \\
& \quad 0 = -P_{B_c,k} + P_{B_d,k} + P_{G_b,k} - P_{G_s,k} + \hat{P}_{PV,k} - \hat{P}_{L,k} \\
& SOC_{min} \leq SOC_k \leq SOC_{max} \\
& \quad 0 \leq P_{B_c,k} \leq P_{B,max} \\
& \quad 0 \leq P_{B_d,k} \leq P_{B,max} \\
& \quad 0 \leq P_{G_b,k} \leq P_{G,max} \\
& \quad 0 \leq P_{G_s,k} \leq P_{G,max}
\end{aligned} \quad (6.13)$$

6.2 Metrics

Evaluating the closed-loop performance is an essential part of developing an MPC scheme. This section aims to develop relevant metrics which can be used in the experiments and address the importance of each metric. All metrics or objectives should be aligned with the overarching goal of the thesis, namely to reduce the cost while securing safe operations.

6.2.1 Operational Costs

The operations costs of the system are cost directly associated with the inputs, selling and buying energy to/from the grid, grid tariff, and battery degradation.

Energy Net Cost - The energy net cost is the net sum of the energy trading with the main grid and is determined by the spot price (Chapter 2.3.1) multiplied with power bought or sold. It is assumed a 10% tax from the TSO when selling to the grid. This results in the following metric for grid cost.

$$\text{Energy Net Cost} = \sum_{i=0}^I E_i(P_{G_{b,i}} - 0.9P_{G_{s,i}}) \quad (6.14)$$

where I is number of time steps in the entire simulation. E_i , $P_{G_{b,i}}$ and $P_{G_{s,i}}$ is the spot-price, grid bought and sold at time-step i , respectively.

Grid tariff - There are two types of grid tariffs, fixed and effect-based. The fixed tariff is defined as following

$$\text{Grid Tariff}_f = \sum_{i=0}^I q_{fixed} P_{G_{b,i}}, \quad (6.15)$$

where again I is the simulation horizon, and $P_{G_{b,i}}$ is electricity bought at time-step i . The effect-based tariff is calculated at the end of the simulation, and is defined as

$$\text{Grid Tariff}_p = q_{peak} G_{P,I}, \quad (6.16)$$

where q_{peak} is the effect-based tariff.

Battery costs - The costs associated with the battery are degradation costs. However, these costs are difficult to estimate and outside the scope of this thesis (Hoel 2020). Therefore the work done by Berg et al. (2021) on the Skagerak Energylab is used for degradation cost, where a linear cost model is assumed inside the operating area. This results in the following cost for the battery.

$$\text{Degradation Cost} = \sum_{i=0}^I C_{deg}(P_{B_{c,i}} + P_{B_{d,i}}), \quad (6.17)$$

where C_{deg} is the battery degradation coefficient.

Furthermore, energy stored in the battery at the end of the simulation should be accounted for in the operational costs. The energy is converted to kWh and multiplied with the spot price at the end of the simulation horizon I .

$$\text{Battery Cost} = E_I(\text{SOC}_{start} - \text{SOC}_{end})C_{max}, \quad (6.18)$$

where SOC_{start} and SOC_{end} is the state of charge at the start and end of the simulation period. C_{max} is the maximum capacity of the battery.

This results in the following expression for operational cost:

$$\text{Operational cost} = \text{Energy Net Cost} + \text{Grid Tariff} + \text{Battery cost} + \text{Degradation Cost} \quad (6.19)$$

where the grid tariff can be either fixed, or effect-based.

6.2.2 Computational Time

If the EMPC should be deployed on the actual power plant, the time used to find a solution must be sufficiently small. The computational time for a single solution starts when measurements are collected and stops when the control actions are calculated. This includes the time it takes to make predictions and select scenarios. In a real-life application, more overhead can be expected, but this is assumed zero. All computational times are calculated with MacBook Pro 16-inch (2019), with a 2.6GHz 6-Core Intel i7 processor.

There are two measures of computational time that are of interest in this thesis, average and worst case. Average computational time is the time it takes on average to solve the OCP at each time step over the entire simulation horizon I . The other measure is the worst-case computational time. This is the solution that took the longest time in the simulation horizon. Both these measures need to be sufficiently small compared to the sampling time for the EMPC to operate smoothly in a real-time situation.

6.2.3 Benchmarks

The benchmarks presented here are used in the case study and provides insight into the performance of the different MPC schemes.

As a *lower benchmark* on performance, a *no-battery controller* is implemented. In a no-battery controller, the goal of the controller is to balance the load and PV power. The balancing is done by exchanging energy with the grid. This is inspired by Kumar et al. (2019), where the authors compare the value of the battery on different MPC schemes.

An *upper benchmark* is also interesting and for this purpose, a deterministic EMPC-scheme with perfect predictions, denoted DEMPC-PP, is used. Perfect prediction is when historical data is used as predictions, and the controller knows the future. This creates a useful upper benchmark for how well the controller can perform.

6.3 Time Series Analysis

This section will detail how the time series used in this thesis was cleaned, analyzed, and predicted. Theory and definitions are explained in Chapter 4.

The relevant time-series are summarized in Table 6.1. The signals used in the MPC scheme are PV generation P_{PV} and load demands P_L .

6.3.1 Data Cleaning

The data used in this thesis was collected from the Skagerak EnergyLab in the period from March 17th to May 7th. The raw data first needed to be cleaned, as each time series had a different sampling rate and time-stamps. Furthermore,

Name	Symbol	Unit	Type
Photovoltaic Power	P_{PV}	kWh	Cumulative
Load Power	P_L	kWh	Cumulative
Air Temperature	AT	$^{\circ}C$	Non-Cumulative
Global Horizontal Irradiance	GHI	W/m^2	Non-Cumulative
Plane of Array Irradiance	PAI	W/m^2	Non-Cumulative

Table 6.1: Time-series used in thesis.

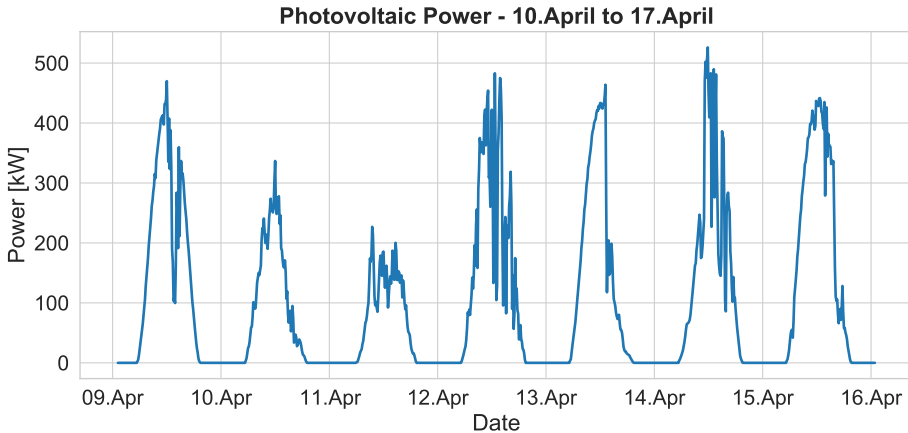


Figure 6.3: Measured P_{PV} plotted over 7 days in April 2021. Collected from Skagerak Energylab.

P_{PV} and P_L is measured cumulatively. Therefore, using the data analysis library Pandas (Pandas 2020), data cleaning was done with the following steps:

1. Interpolate missing values.
2. Re-sample the data to 10-minute resolution. The non-cumulative TS was aggregated with the mean over the 10 minutes, while the cumulative used the last measured value.
3. The cumulative TS was made non-cumulative by subtracting the value at time t with the value at $t - 1$. Furthermore, all values with unit kWh were divided with $\frac{10\text{minutes}}{60\text{minutes}/\text{hour}}$ to get the correct unit kW.

At the end of the data cleaning, all of the time series were non-cumulative, with equal time-stamps and corresponding units.

6.3.2 Photovoltaic Forecasting

Figure 6.3 is a snippet from the data set and shows the measured power production from the PV-cells over a week in April. To develop accurate prediction methods for PV production, data over a whole year is desirable to catch seasonal differences. However, this was not available for this thesis work. By observation, P_{PV} is periodic, which can be expected as solar production follow the cycle of the sun. Furthermore, the production can have large fluctuations, which can be seen on, for example, April 13th. The source for this behavior is most likely cloudy weather that blocks the sun. There are no apparent trends in P_{PV} in this plot, but seasonal differences between summer and winter should be expected.

Feature- and auto-correlations are calculated to understand the time series better and discuss which forecasting method best suits the problem. In Figure 6.4, the correlation between the time-series available is plotted. The first columns show the PV correlation coefficients and show high values with global horizontal irradiance (GHI) and the plane of array irradiance (PAI). Also, there is some correlation between the air temperature (AT) and the load. These findings have also been found in Chen et al. (2020). Since PAI is highly correlated with GHI, the information relevant to predicting PV power is already incorporated into GHI. AT and GHI are used in the prediction methods, as these contain the most information, and numerical weather predictions are available.

Furthermore, the auto-correlation for one day is plotted in Figure 6.5. From the plot, periodic behavior can be observed, which is expected due to the day and night variation and can also be seen in Figure 6.3. Furthermore, a high correlation is seen between the first samples. This means that the current value can contain information about the following values, so the prediction method should utilize the ability to measure the signals at each time step.

Based on Figure 6.4 and Figure 6.5, we propose to use a method that relies on current measurement for short term prediction, and features for the long term predictions.

The available data was divided with a 50-50 split into two separate sets, denoted training set and test set, to evaluate the methods. The methods are not exposed to the test set during training, and unless otherwise stated, the test set is used.

Prediction Pipeline

Step 1 - Collecting Numerical Weather Predictions NWP are collected from the third-party company called Solcast (Solcast 2021), which updates their forecasts every hour. Figure 6.7 shows a typical forecast, which also provides the 10th and 90th percentiles for the predictions.

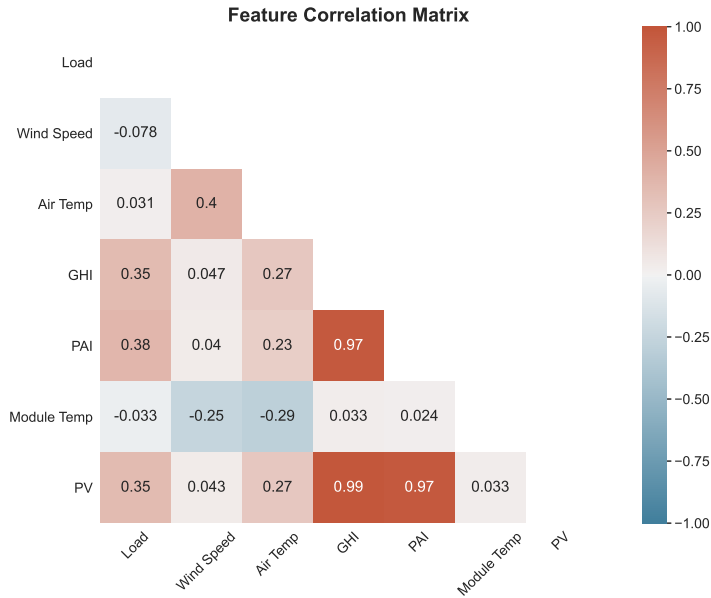


Figure 6.4: Correlation between features. PV - Photovoltaic Power, GHI - Global Horizontal Irradiance, PAI - Plane of Array Irradiance.

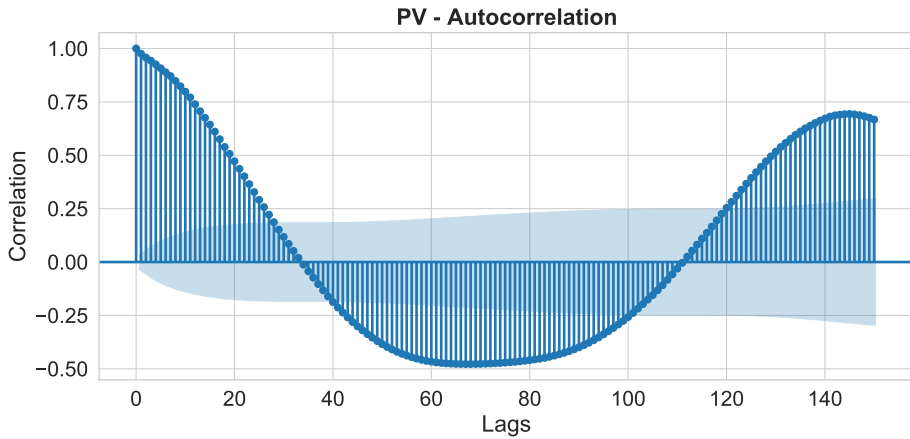


Figure 6.5: PV Auto-correlation over 144 lags, which is one day with 10 minute resolution. The bars represent correlation with first sample, and the blue shaded area is the 95% confidence interval.

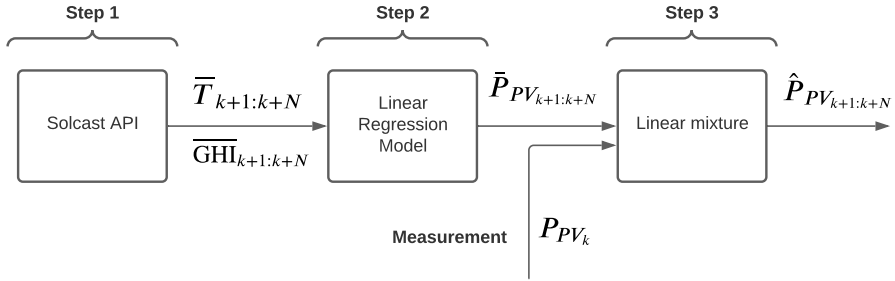


Figure 6.6: Prediction pipeline from numerical weather predictions to PV-prediction.

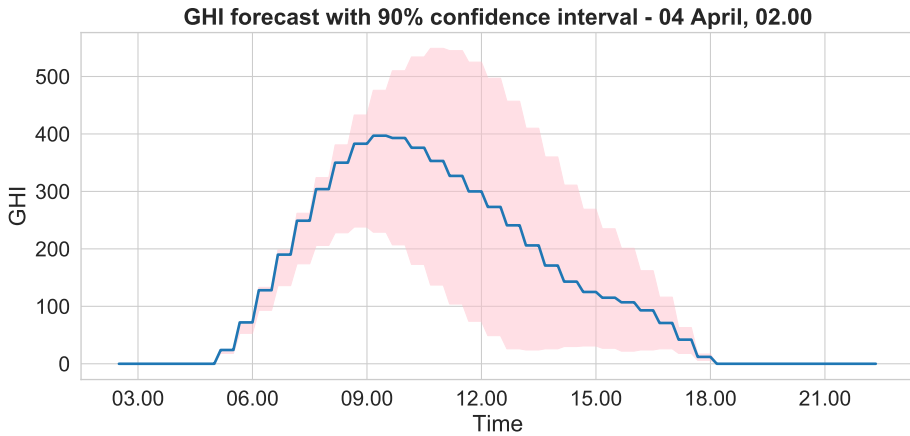


Figure 6.7: Example of Solcast forecast. The blue line is the main prediction, and the shaded red area is between 10th and 90th percentile value.

A *mean prediction* is used as a baseline in this step to evaluate the numerical weather prediction. A mean prediction entails calculating the average day of the observed values in the training set and using it as the prediction. The resulting root mean squared errors (Chapter 4.1) are shown in Table 6.2. The RMSE is still high, though this is due to the noisy real-world signals, shown in Figure 6.3.

Step 2 - Feature-based Method Two methods were examined for predicting P_{PV} based on NWP, multiple linear regression (MLR), as described in Chapter 4.2.1, and a mathematical model (Chapter 4.2.4). The features selected were GHI and

Signal	Metric	Baseline	Solcast	Improvement
GHI	A-RMSE	125.8 W/m ²	91.4 W/m ²	27.3 %
GHI	1-RMSE	110.1 W/m ²	84.8 W/m ²	23.0 %
AT	A-RMSE	3.71 °C	2.41 °C	35.0 %
AT	1-RMSE	3.52 °C	2.01 °C	42.8 %

Table 6.2: Comparison of Solcast and baseline forecasts. A-RMSE is calculated with 10h prediction and 1-RMSE is the one-step RMSE over the test-period.

Metric	MLR	PV-Model	Improvement
A-RMSE	10.3 kW	8.7 kW	15.5 %
1-RMSE	8.9 kW	7.3 kW	18.0 %
Computational time	0.6 ms	291 ms	-

Table 6.3: Comparison of Multiple Linear Regression (MLR) and mathematical PV-model. Computational time is calculated as the average computational time per prediction. A-RMSE and RMSE₁ are the root mean square error over a 10h prediction horizon and the first step respectively.

AT, as these are a part of the mathematical expression in Equation 4.9. MLR was implemented with the Python package SciKit-Learn (Pedregosa et al. 2011) and trained with the observed values in the training set. The PV model was implemented with Casadi (Andersson et al. 2012). Both methods were evaluated on the observed values in the test set for GHI and AT for comparison. The results are summarized in Table 6.3.

Table 6.3 shows that the mathematical PV model is better than MLR, both over the entire prediction horizon and at the first prediction step. The main difference between the methods is in computational time, although both are insignificant to the MPC sampling time of 10min. Furthermore, if comparing the errors in Table 6.2 and Table 6.3, the errors caused by the weather predictions far exceed the errors caused by the prediction method. Therefore, the method chosen is MLR.

Step 3 - Linear Mixture Following the discussion based on the auto-correlation (Figure 6.5), the one-step error 1-RMSE can be reduced by utilizing the measurement. A method is to weigh the measurement more heavily early in the prediction horizon and gradually trusting the feature-based method further in the future. Linear mixture was implemented using the two functions shown in Figure 6.8. After 16 time-steps (2.5 hours), only the feature-based predictions are used, and 16 was chosen as auto-correlation was still high (Figure 6.5).

Table 6.4 shows the errors with and without linear mixture when using numerical weather predictions and MLR. There is a significant improvement in one-step predictions, which also gives a slight improvement in A-RMSE.

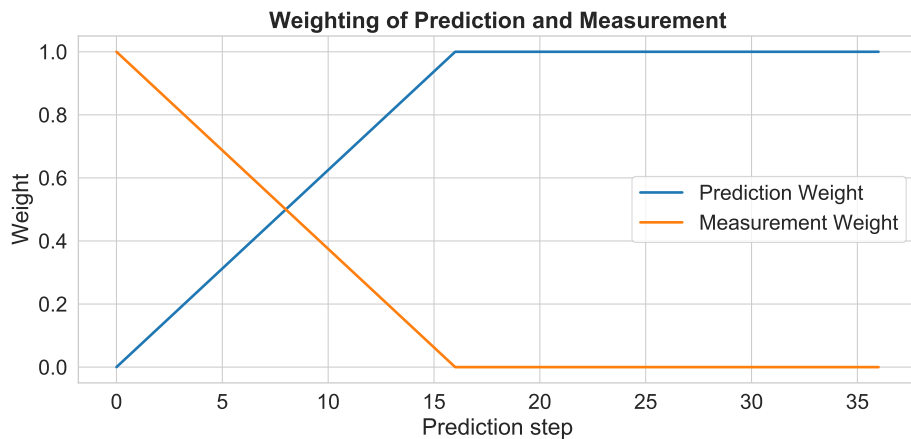


Figure 6.8: The two weight functions used in to combine measurement and prediction.

RMSE Type	Without LM	With LM	Improvement
A-RMSE	46.1 kW	43.6 kW	5.4 %
1-RMSE	55.0 kW	31.5 kW	42.7%

Table 6.4: Comparison of Multiple Linear Regression P_{PV} predictions with and without linear mixture (LM).

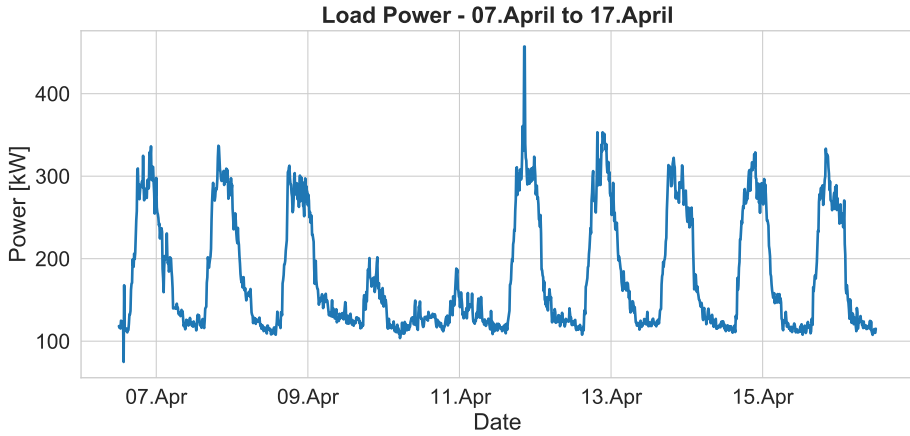


Figure 6.9: P_L plotted over a 10 day period in April. Collected from Skagerak Energylab.

6.3.3 Load Forecasting

Figure 6.9 shows a plot of the load time-series for 10 days in April. The plots show periodic behavior, although with different behavior on April 10th and April 11th. This is most likely due to less activity on the weekend. As with P_{PV} , there does not seem to be a trend that affects the load, but it will decrease in summer and increase in winter due to heating. Furthermore, there appears to be some noise in the time series.

Based on Figure 6.9, *knowledge-based* predictions is used with two clusters in which a day can belong to; weekday or weekend. This method was inspired by Labeeuw & Deconinck (2013), which creates clusters from thousands of residential houses. The clusters are updated every day and collect the days from the three previous weeks. The predictions are then calculated by taking the average of the relevant cluster. The averaging is performed to remove noise and outliers, for example, the one that occurs on April 12th.

The load auto-correlation in Figure 6.10 looks similar to the P_{PV} , which is expected due to the period behavior. The high auto-correlation early also suggest using the linear mixture method that was used to predict P_{PV} . The results of the prediction method are shown in Table 6.5, and significant improvement can be seen when using the linear mixture.

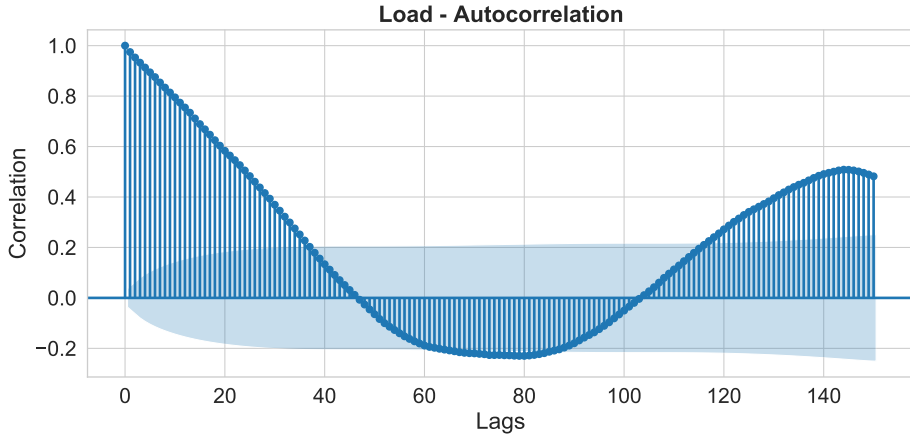


Figure 6.10: Load auto-correlation over 144 lags, which is one day with 10 minute resolution. The bars represent correlation with first sample, and the blue shaded area is the 95% confidence interval.

RMSE Type	Without LM	With LM	Improvement
A-RMSE	52.1 kW	49.4 kW	5.2 %
1-RMSE	50.1 kW	13.0 kW	74.1 %

Table 6.5: Comparison of P_L predictions with and without linear mixture (LM).

6.4 Handling Uncertainty

As can be seen in Table 6.4 and Table 6.5, the predictions are far from perfect. These uncertainties are modeled by redefining the signals P_{PV} and P_L as following

$$P_{PV} = \hat{P}_{PV} + \tilde{P}_{PV}, \quad (6.20a)$$

$$P_L = \hat{P}_L + \tilde{P}_L, \quad (6.20b)$$

where \hat{P}_{PV} and \hat{P}_L are the predicted PV and load signals. The uncertainties \tilde{P}_{PV} and \tilde{P}_L are stochastic variables with unknown probability distributions ϕ_{PV} and ϕ_L . The error or *effective disturbance* on the system is the difference $e = \tilde{P}_{PV} - \tilde{P}_L$, which comes from the topology constraint (Equation 6.1). In our simulations, the effective disturbance is fixed with a *recourse action*. It can be viewed as a primary controller which steps in after the energy management system has failed to balance the power and demand. The power balance is restored by trading energy with the main grid.

ϕ_{PV} and ϕ_L are estimated using the *kernel density estimation* (KDE), which uses observed data to approximate a probability distribution. KDEs are calculated by first collecting the observed error into bins, resulting in a *histogram*. Then the histogram translated into a continuous function by approximating each bin with kernel. Choosing the correct kernel is necessary to get a good estimate of the probability distribution. To implement the KDE, we used the Python package Scipy (Virtanen et al. 2020), which automatically finds the best kernel.

Both the marginal and joint KDE of ϕ_{PV} and ϕ_L is shown in Figure 6.11. Since there is no solar production at night, $\tilde{P}_{PV} = 0$ in these hours. Then the joint KDE reduces to the marginal distribution of \tilde{P}_L , and are therefore left out of Figure 6.11.

Since the effective disturbance appears as the difference between \tilde{P}_{PV} and \tilde{P}_L , the extreme scenarios appear when the two signals are oppositely large. Figure 6.11 shows these scenarios in the upper left corner if PV prediction overestimates and the load prediction underestimates, and the lower right corner where the opposite happens. However, the KDE plot shows that the likelihood of that happening is relatively low.

6.4.1 Scenario-tree EMPC

\tilde{P}_{PV} and \tilde{P}_L are modeled as scenarios and will be detailed in the next section. They reflect different realizations of the uncertainty and can be included in a scenario-tree formulation as discussed in Chapter 5.4. Because computational speed is relevant in this context, the approximated scenario-tree scheme that was discussed in Chapter 5.4.4 is used.

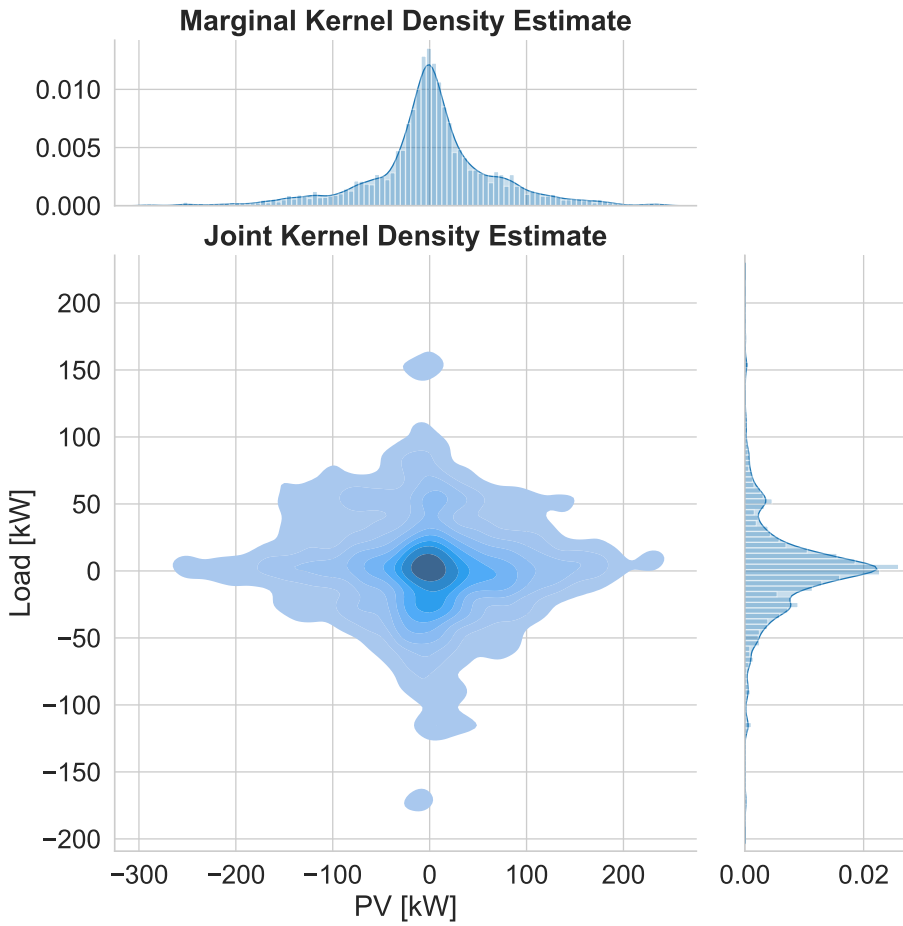


Figure 6.11: Marginal and joint kernel density estimate of \tilde{P}_{PV} and \tilde{P}_L . Darker color suggests a higher density in the joint KDE plot.

$$\min_{x_j, u_j} \sum_{j=0}^S w_j \left[\sum_{k=0}^{N-1} \ell_B(u_{j,k}) + \ell_{G_m}(u_{j,k}) + V(x_{j,N}) \right], m \in \{p, f\} \quad (6.21a)$$

$$s.t. \quad SOC_{j,k+1} = \frac{\eta_c P_{B_c,j,k}}{C_{max}} - \frac{P_{B_d,j,k}}{\eta_d C_{max}} \quad (6.21b)$$

$$\begin{aligned} G_{P,j,k+1} &\geq G_{P,j,k} \\ G_{P,j,k+1} &\geq P_{G_b,j,k} \end{aligned} \quad (6.21c)$$

$$\begin{aligned} 0 &= -P_{B_c,j,k} + P_{B_d,j,k} + P_{G_b,j,k} \\ &\quad - P_{G_s,j,k} + \hat{P}_{PV,j,k} - \hat{P}_{L,j,k} \end{aligned} \quad (6.21d)$$

$$SOC_{min} \leq SOC_{j,k} \leq SOC_{max} \quad (6.21e)$$

$$0 \leq P_{B_c,j,k} \leq P_{B,max} \quad (6.21f)$$

$$0 \leq P_{B_d,j,k} \leq P_{B,max} \quad (6.21g)$$

$$0 \leq P_{G_b,j,k} \leq P_{G,max} \quad (6.21h)$$

$$0 \leq P_{G_s,j,k} \leq P_{G,max} \quad (6.21i)$$

$$P_{B_c,j,0} = P_{B_c,l,0} \quad j, l \in [0, 1, \dots, S], j \neq l \quad (6.21j)$$

$$P_{B_d,j,0} = P_{B_d,l,0} \quad j, l \in [0, 1, \dots, S], j \neq l \quad (6.21k)$$

The equations in 6.21 show the resulting scenario-tree OCP, where S is the number of scenarios. The cost-function Equation 6.21a is the accumulated cost over all scenarios weighted with w_j , which will be discussed in the next section. Equation 6.21b and Equation 6.21c, shows the state evolution of SOC and grid peak respectively. Equation 6.21e-Equation 6.21i shows the constraints in the system.

However, the formulation above is different from what was discussed in Chapter 5.4, in the sense that the disturbances occur in the topology constraint and not in the differential equation. This creates an issue with the non-anticipativity constraints. Different realizations of the uncertainty require a unique combination of inputs to satisfy the topology constraint. If all the first inputs are forced to be equal between the scenarios, this will result in an infeasible problem. Therefore only the battery inputs P_B has non-anticipativity constraints, as shown in Equation 6.21j and Equation 6.21k. As a result, the grid inputs can vary between the scenarios to make sure the topology constraint is maintained and the problem remains feasible.

6.4.2 Selecting Scenarios

Following the discussion in Chapter 6.4, the scenarios can be chosen either in a robust or stochastic fashion. Figure 6.11 the estimates of the probability distributions ϕ_{PV} and ϕ_L . However, creating discrete scenarios from ϕ_{PV} and ϕ_L require computationally expensive methods, for example, Monte Carlo simulations and

scenario-reduction.

Therefore, a relaxed robust formulation with soft bounds on the uncertainty is used, inspired by Carli et al. (2020). This entails creating an upper and lower bound on \tilde{P}_{PV} and \tilde{P}_L , but it does not require the set to contain the most extreme values of the uncertainty. Due to the primary controller, there will never be severe constraint violations, and an extremely conservative controller is unnecessary. However, the grid peak G_P is modeled as a soft constraint. Breaking the constraint comes with an economical penalty and a robust formulation will therefore be able to reduce the cost.

Scenarios

The scenarios for P_{PV} are created from the interval between the 10th and 90th percentile provided along with the main predictions collected from Solcast (2021). These can be seen in Figure 6.7, and are illustrated as the edges of the red shaded area. The optimistic and pessimistic scenarios are denoted $P_{PV,upper}$ and $P_{PV,lower}$ respectively. Together with the main prediction \hat{P}_{PV} , we get three scenarios for PV. An example of a cloudy day is shown in the top plot in Figure 6.12, where the predictions and scenarios are plotted at 00.00 and 10.00. The jump at 10.00 is due to updated weather forecasts and linear mixture. Though the clouds give a noisy behavior, the observed value is usually inside the interval between $P_{PV,upper}$ and $P_{PV,lower}$.

The scenarios for P_L are created similar to the predictions (Chapter 6.3.3), where weekdays and weekends are separated. Then, based on the previous three weeks, the day with the highest and lowest load demands are used as upper $P_{L,upper}$ and lower $P_{L,lower}$ scenario, respectively. Again this results in three scenarios, which are shown in the lower plot in Figure 6.12. In this plot, the prediction is quite good, and $P_{L,upper}$ provides a reasonable upper bound for the uncertainty. However, $P_{L,lower}$ is a conservative scenario, which can happen if there are holidays or days where the Skagerak EnergyLab is not active in the previous three weeks. Better methods for generating these scenarios can be researched further, but an acceptable performance was achieved using this method.

Three scenarios for both P_{PV} and P_L gives nine possible combinations. Following the discussion from Chapter 6.4, the extreme combinations of scenarios happens in the upper left or lower right corner in Figure 6.11. In contrast, the errors will cancel each other out in the lower left and upper right corners. In Figure 6.13 the KDE of \tilde{P}_{PV} and \tilde{P}_L is plotted with an optimistic and a pessimistic scenario. The optimistic scenario is the event of $P_{PV,upper}$ and $P_{L,lower}$, and the pessimistic scenario the opposite $P_{PV,lower}$ and $P_{L,upper}$. The optimistic and pessimistic scenarios have estimated densities that are shifted such that they cover the uncertainty of the original prediction.

Three different scenario-tree EMPCs are compared in this thesis; 3, 7, and 9 branches denoted SEMPC-3, SEMPC-7, and SEMPC-9. SEMPC-3 contains the

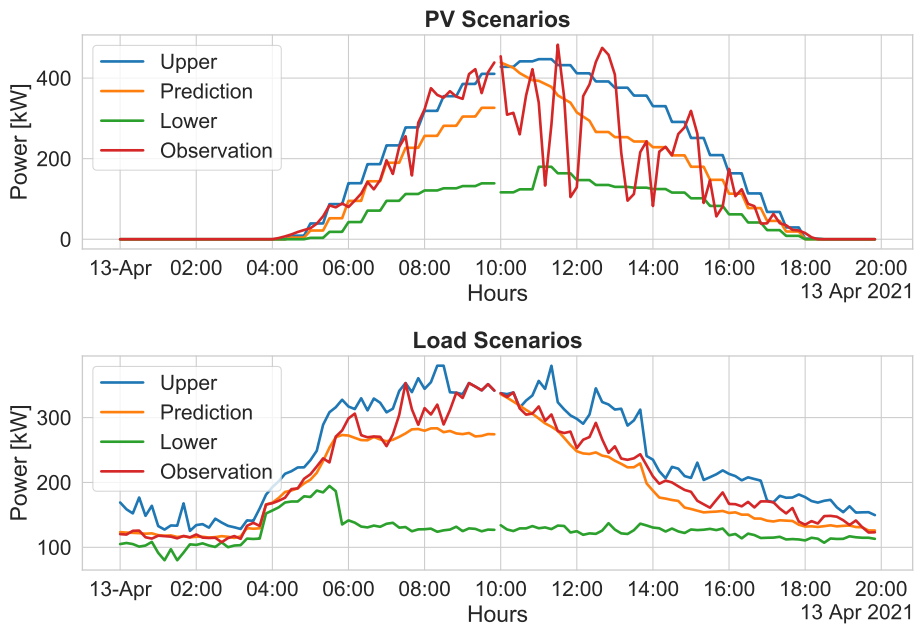


Figure 6.12: Comparison of predictions, scenarios, and observation on April 13th. Predictions and scenarios are plotted at 00.00 and 10.00, with a 10 hour prediction horizon.

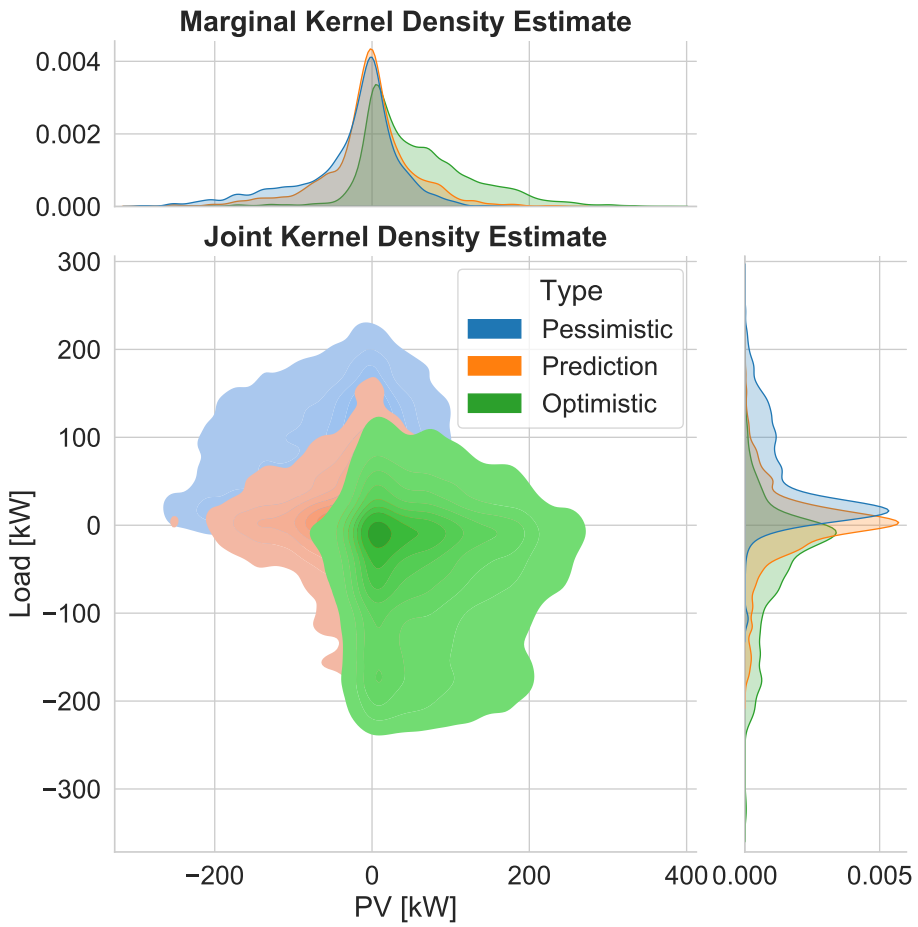


Figure 6.13: Kernel distribution estimates of the uncertainties in the original prediction method \tilde{P}_{PV} and \tilde{P}_L , together with optimistic and pessimistic scenarios.

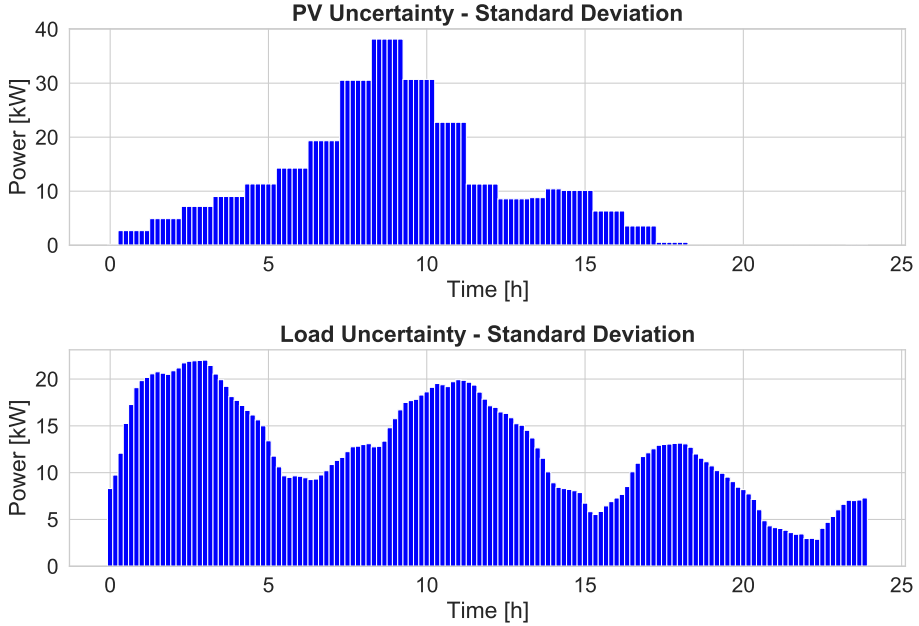


Figure 6.14: Standard deviation of prediction error given time-of-day for the uncertainties \tilde{P}_{PV} and \tilde{P}_L .

predictions as well as an optimistic and a pessimistic scenario as shown in Figure 6.13. SEMPC-9 includes all nine combinations of the scenarios, while the SEMPC-7 has only left out $P_{L,lower}-P_{PV,lower}$ and $P_{L,upper}-P_{PV,upper}$, since these are scenarios where the disturbances cancels each other out.

Weighting

Next, the weighting w_j for each scenario has to be calculated based on the probability distributions Φ_{PV} and Φ_L of the uncertainty. To do this, we make use of another component; time. Since both P_{PV} and P_L are non-stationary signals, Φ_{PV} and Φ_L are dependent on time. This can also be seen in Figure 6.12, and especially in P_{PV} , where the power generated varies greatly during the day and is always zero at night. This is demonstrated in Figure 6.14, where the standard deviation of \tilde{P}_{PV} and \tilde{P}_L is plotted. Higher standard deviations at certain times suggest the prediction method gives worse forecasts and less trust in the prediction around these times.

6.5 Methodology Summary

This chapter started by formulating an optimal control problem for the Skagerak EnergyLab used in a controller. Which further resulted in a deterministic EMPC with two different price models for grid tariff. Next, the prediction methods for P_{PV} and P_L were developed, where the predictions \hat{P}_{PV} are calculated using numerical weather predictions and multiple linear regression. The load predictions \hat{P}_L are based on a knowledge-based system, where days are separated into two clusters; weekday and weekend. Both predictions were also passed through a linear mixture to reduce the one-step error, which is beneficial for the EMPC-scheme.

Next, the prediction errors \tilde{P}_{PV} and \tilde{P}_L were investigated, and a scenario-tree formulation was developed to model the uncertainties into the EMPC scheme. Then the scenarios were presented with the calculation of probabilities for each scenario based on available data. The scenarios were chosen to cover the uncertainty, and by using the time component, probabilities was calculated for each time step of the day.

Results

The deterministic EMPC implemented is based on the one used in the project thesis Husefest (2020). However, it has been greatly improved upon, both by parameter tuning and new prediction methods. Further, all results are obtained from the code developed throughout this thesis work. The code was programmed in CasADi Andersson et al. (2012) were the systems given by 6.13 and 6.21 were implemented.

This chapter presents the results obtained throughout this thesis. Experiment 1 shows the effect of terminal cost on the EMPC scheme, which is previously discussed in Chapter 6.1. Afterward, the economic performance of the EMPCs are evaluated. Since there are two different economic situations, these will be presented separately. Experiment 2 shows the performance with a fixed grid tariff, while experiment 3 presents the effect-based tariff. Both experiments 2 and 3 are tested over 30 days, from April 7th to May 7th, in order to get a realistic impression of the monthly costs. Snippets of the simulation are presented with comments on the behavior of the different EMPC-schemes. The spot prices are assumed known since the day-ahead market decides the price and closes around 24 hours beforehand. All other constants used in the experiments are summarized in Table 7.1.

7.1 Experiment 1 - Terminal Cost

The importance of a terminal cost in an EMPC-scheme is discussed in Chapter 5.3.3, and is demonstrated in this section. The optimal terminal cost used is calculated with the method described in Chapter 6.1.5.

The EMPC scheme used is a deterministic EMPC scheme with a fixed grid tariff and perfect predictions. Ideally, an infinite horizon would be used. However, the longest prediction horizon that was computationally feasible was 72 hours, which is 432 steps with a sampling time of 10 minutes.

The three configurations used in the experiment are summarized in Table 7.2. Configuration a) tries to approximate an infinite horizon by having a long pre-

Symbol	Description	Value
I	Simulation Horizon	30days / 720 hours
Ts	Sampling Rate	10Min
N	Prediction Horizon	6 hours
C_{max}	Maximum capacity of battery storage system	1100 kWh
η_c	Battery charge coefficient	0.91
η_d	Battery discharge coefficient	0.91
$P_{G,max}$	Maximum power to/from the grid	1000kW
$P_{B,max}$	Maximum power to/from the battery	800kW
SOC_{min}	Minimum state of charge	20%
SOC_{max}	Maximum state of charge	80%
C_{deg}	Battery degradation coefficient	0.064NOK/kWh
q_{fixed}	Consumption/fixed based grid tariff	0.36NOK/kWh
q_{peak}	Effect based grid tariff	51 NOK/kW/month

Table 7.1: Parameters used in the experiments. The charge and discharge coefficients η_c and η_d were calculated in the project thesis by Hoel (2020). C_{max} , $P_{G,max}$, $P_{B,max}$, C_{deg} , q_{fixed} and q_{peak} are collected from the economic evaluation of the Skagrag EnergyLab in Berg et al. (2021). SOC_{min} and SOC_{max} are based on the assumption on linear working area for the battery and degradation, discussed in Chapter 3.4.3.

diction horizon and no terminal cost. b) uses a six-hour prediction horizon, but no terminal cost, while c) has an optimal terminal cost, which was found to be $V(x_N) = -812SOC$. The negative coefficient translates to rewarding a high state of charge.

In Figure 7.1, the DEMPC with a short prediction horizon and no terminal-cost (configuration b) is more willing to deplete the battery and is, therefore, more often at a lower state of charge. This strategy provides less flexibility later in the day, where it is forced to buy electricity at a higher price than the two other configurations. This gives a slightly higher operational cost in this example. The two configurations a) and c) follow each other more closely and are more conservative using the battery. Table 7.2 shows that short prediction horizon and terminal cost have a lower operational cost than long prediction horizon. However, two days is not enough to conclude that this is true in general. The most significant difference is the computational time, where configuration b) and c) are magnitudes faster than a). Therefore, we can say that the terminal cost significantly reduces computational time over these two days without a loss in performance.

Configuration	Hours	N	Terminal Cost	Average Computational Time	Operational Costs
a)	72	432	No	1.94s	1848.6 NOK
b)	6	36	No	0.053s	1938.0 NOK
c)	6	36	Yes	0.048s	1840.6 NOK

Table 7.2: Parameters used in the different configurations and corresponding results. Operational costs from the period April 13th to April 15th, with 10 minute sampling time.

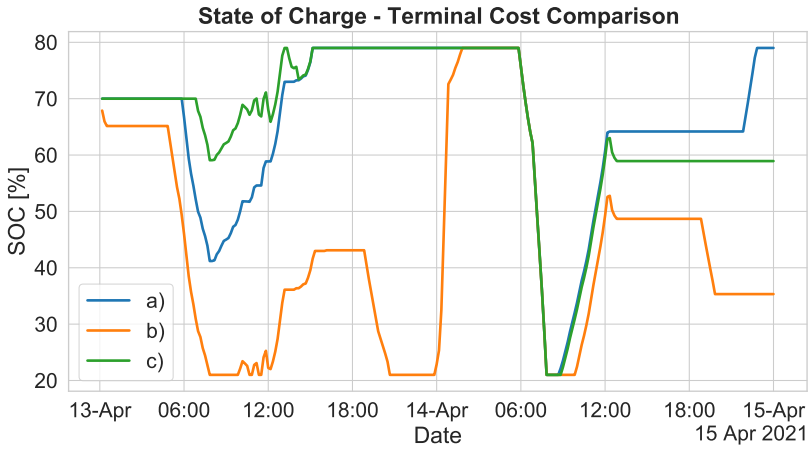


Figure 7.1: Comparison of terminal costs, given configurations a) - long prediction horizon - no terminal cost, b) - short prediction horizon - no terminal cost and c) - short prediction horizon - with terminal cost.

	Grid Tariff Cost	Energy Net Cost	Total Costs
DEMPC-PP	18914 NOK	3141 NOK	22536 NOK
No Battery	22249 NOK	21110 NOK	43359 NOK

Table 7.3: Operational costs for the 30 days simulation with DEMPC and no-battery controller.

7.2 Experiment 2 - Fixed Tariff

In this experiment, the EMPC-schemes are tested with the consumption-based fixed grid tariff. This means the OCP in Equation 6.13 is used with the grid-costs as in Equation 6.8. First, the performance of the deterministic EMPC with perfect predictions (DEMPC-PP) is tested before uncertainties are included. Then the performance of DEMPC with uncertainties is compared to the SEMPC, which uses the OCP in Equation 6.21 with the fixed grid tariff (Equation 6.8).

7.2.1 Experiment 2.1 - Fixed Tariff, Perfect Predictions

To show how the DEMPC-PP behaves, a two-day snippet from the month simulation is extracted in Figure 7.2. These days were chosen because the spot prices (Figure 7.2c) varies more than usual. The grid and battery usage is plotted in Figure 7.2a), where negative grid means selling, and negative battery values are equivalent with discharging. In Figure 7.2b) the SOC is plotted.

In Figure 7.2a), there is no power sold to the grid due to the extra cost of selling. This leads to storing and load covering being the optimal solution, despite the battery losses, where some energy is lost when charging and discharging, and degradation cost, discussed in Chapter 6.10. This means that buying energy for the purpose of selling it later requires a larger difference in spot prices than observed in this example. However, it still uses the battery to reduce operational costs by covering the load. In the mornings on both April 7th and 8th, energy is bought cheap to charge the battery. As spot prices increase around 06.00, the controller uses the battery to cover the load and avoid buying expensive electricity. Around 12.00, as PV production surpasses load demands (Figure 7.2d), the DEMPC-PP finds it optimal to use excess PV production to charge the battery.

DEMPC-PP was earlier introduced as an upper benchmark, and in table 7.3 it is compared to the lower benchmark, the cost of the system with no battery, for a 30 days simulation. The cost of these two systems differs greatly and highlights the need for an efficient micro-grid with a battery and a controller. The main difference between the two controllers is in energy net cost, meaning that DEMPC-PP can take advantage of the differences in spot prices.

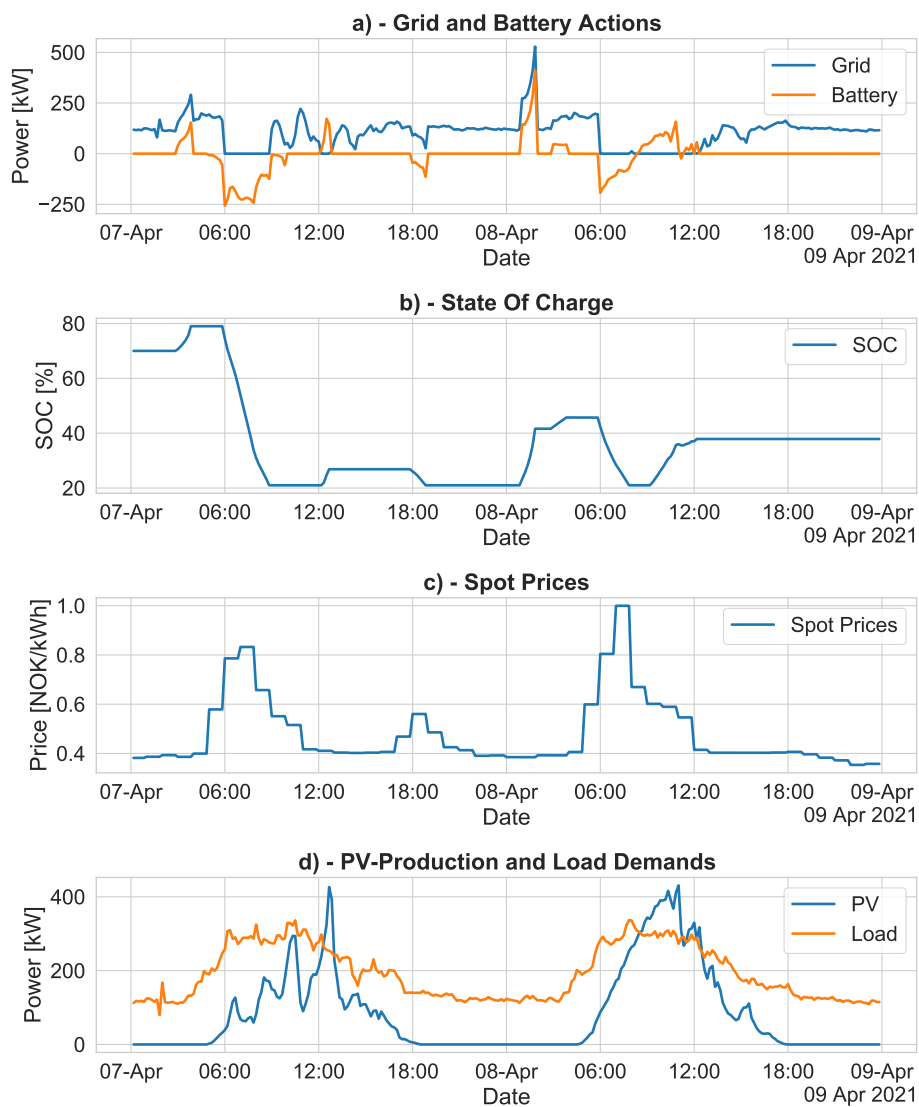


Figure 7.2: Snippet (April 7th to 9th) from experiment 2.1 - Fixed grid tariff and perfect predictions. Subplot a) shows the grid and battery actions, b) shows the state of charge, c) spot-prices and PV-production and load demands in d).

7.2.2 Experiment 2.2 - Uncertainties

In this experiment, perfect predictions are no longer assumed, and the prediction methods discussed in Chapter 6.3 are used instead. Recall that the *effective disturbance* is defined as the difference $\tilde{P}_{PV} - \tilde{P}_L$, which is the errors corrected by the primary controller.

The benchmark is the DEMPC with perfect predictions (DEMPC-PP), which is compared to DEMPC without perfect predictions, as well as the three configurations of SEMPC, discussed in Chapter 6.4.

In Figure 7.3, April 15th is extracted from the 30day simulation, since this was a cloudy day with high variance in PV-production, which can be seen in Figure 7.4. In Figure 7.3a), the grid actions are shown. Both DEMPC and SEMPC-9 fluctuate more than DEMPC-PP, which can to some degree be explained by the influence of the primary controller, which corrects the effective disturbance (Figure 7.3d). Positive disturbance corresponds to a surplus of energy, and negative a deficit. Around 12.00, large spikes in the effective disturbance are corrected by selling or buying energy. The DEMPC-PP is able to use all the PV production for charging the battery, but the disturbances force the primary control to sell energy at a relatively low price for both DEMPC and SEMPC. Therefore the DEMPC-PP is able to fully recharge the battery in (Figure 7.3b), which is sold to a higher price around 18.00.

However, in the morning, the three controllers behave differently. Neither DEMPC nor SEMPC-9 follows DEMPC-PP, even though the disturbance is low. This is the consequence of poor predictions, which can be seen in Figure 7.4. In the morning, the predictions overestimate P_{PV} , and the DEMPC expects that it can use that energy to cover the load without buying from the grid. As it gets closer to the peak in spot price at 06.00, the predictions get better, and it rushes to purchase energy. However, the price has already started to increase, and the controller is forced to buy energy at a slightly higher price than DEMPC-PP. The SEMPC-9 also expects it can cover the load. However, as the controller realizes this is not the case, but unlike the DEMPC, it maxes out the grid right before the spot prices increase.

Table 7.4 summarizes the performance of the controllers with fixed tariff. All of the EMPC schemes have a significant increase in performance compared to the no-battery controller. Furthermore, there is a slight difference between DEMPC and SEMPC, where the DEMPC has the lowest operational cost. This is because even though the DEMPC sometimes ends up buying energy at a higher price, it does not severely affect the total costs. However, the conservative approach of the SEMPC with buying a lot of energy before periods with high uncertainty results in a higher total cost due to the battery cycle's losses. Over a full month, the three EMPC schemes seem to give approximately the same cost.

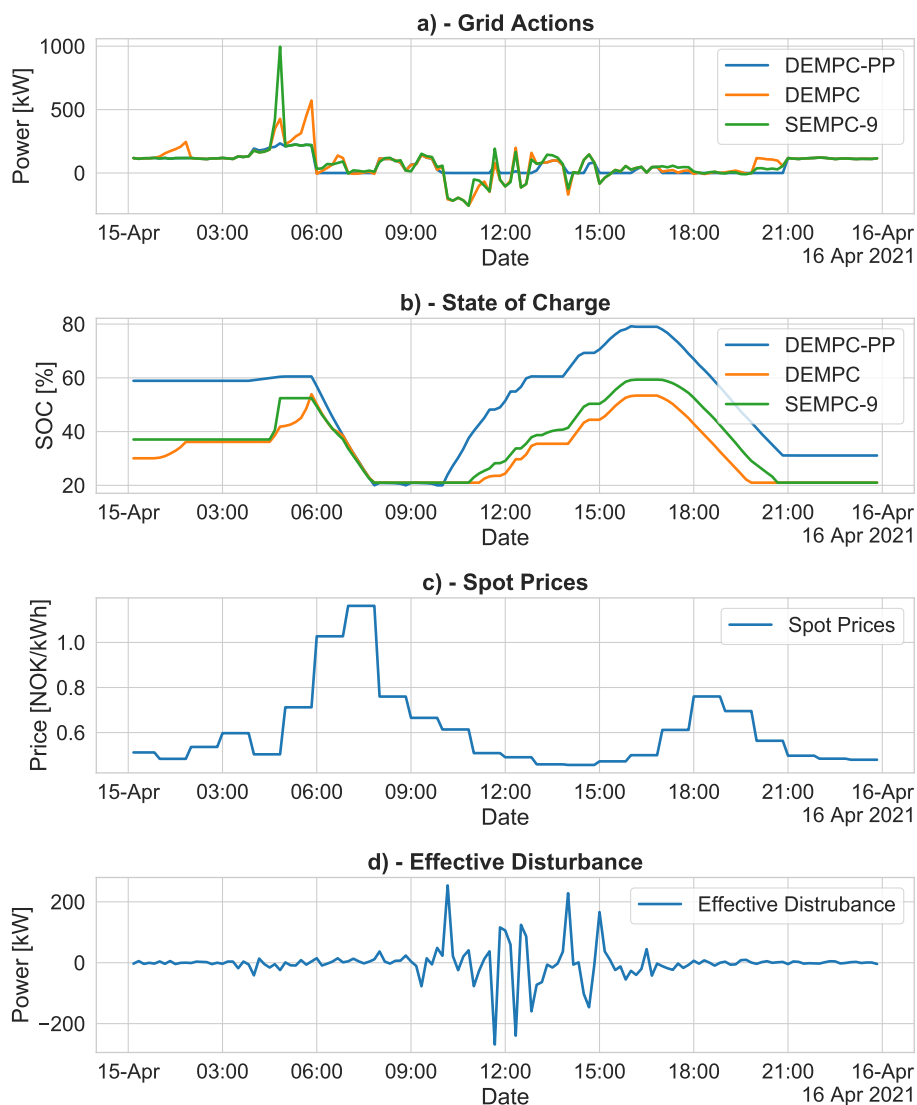


Figure 7.3: Snippet (April 15th to 16th) from experiment 2.2 - Fixed tariff for the DEMPC-PP, DEMPC and SEMPC-9. Subplot a) shows the grid and battery actions. Subplot b) shows the state of charge, spot-prices are plotted in c) and PV-production and load demands in d).

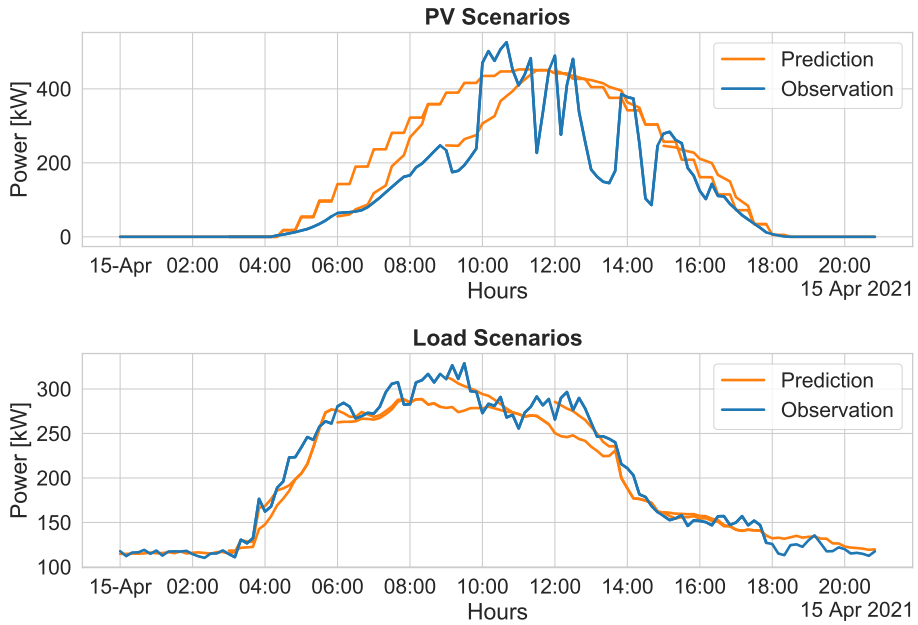


Figure 7.4: Predicted and observed values for P_{PV} and P_L on April 15th. Predictions are plotted every third hour and with a six hour horizon.

	Operational Costs	Improvement	Average Comp. Time	Worst Case Comp. Time
No Battery	43359 NOK	-	-	-
DEMPC-PP	22536 NOK	48.0%	0.042s	0.108s
DEMPC	23003 NOK	47.0%	0.041s	0.121s
SEMPC-3	23091 NOK	46.9%	0.138s	0.276s
SEMPC-7	23149 NOK	46.6%	0.330s	1.32s
SEMPC-9	23224 NOK	46.4%	0.370s	1.45s

Table 7.4: Comparison of the different EMPC-schemes using fixed grid tariff. DEMPC with perfect predictions is used as benchmark for percentages.

	Grid Tariff Cost	Energy Net Cost	Total Costs
DEMPC-PP	8007 NOK	3111 NOK	11275 NOK
No Battery	15249 NOK	21110 NOK	36359 NOK

Table 7.5: 30 days simulation with DEMPC and the system with no battery.

7.3 Experiment 3 - Effect Based Tariff

Next, the effect-based tariff is used. This means using the OCP in Equation 6.13, with the peak-power cost function (Equation 6.9) in the EMPC schemes. Snapshots are presented with comments on the behavior, while the operational costs are calculated over a month.

7.3.1 Experiment 3.1 - Perfect Predictions

The introduction of peak cost changes the behavior of the MPC, as can be seen in Figure 7.5, which shows the first two days in the simulation period. To keep the peak low, the DEMPC-PP finds it optimal to consistently buy energy at a low peak value, as long as the spot prices are relatively low. In the morning on April 8th, the spot-prices increase, and therefore the DEMPC-PP uses the battery (Figure 7.5b)) and PV-production to cover the load. As power production surpasses the load demands (Figure 7.5d)), the energy is used to charge the battery.

In table 7.5 the DEMPC-PP is compared with the lower benchmark, which is the cost of the system with no battery. With the effect-based tariff model, the advantages of peak shaving with a battery are highlighted. Without using a battery, the largest peak is decided by the maximum difference between the production and the demand. This creates an arbitrary peak cost that can change widely from one month to the next. With a battery, the micro-grid can perform peak shaving to save on cost while still using the battery for load covering and energy trading. The result is a monthly cost of only a third of the system with a no-battery controller.

7.3.2 Experiment 3.2 - Uncertainties

Next, uncertainties are introduced into the system with an effect-based tariff. In the previous section, the controller was able to minimize the grid peak when having perfect predictions. However, DEMPC-PP usually operates close to or on the current peak values, and with disturbance, the primary controller may push the peak upwards.

Figure 7.6 shows the evolution of the peak over the test month. As expected, DEMPC-PP keeps the peak far lower than the other EMPC-schemes. Furthermore, the SEMPC-7 and SEMPC-9 keep the peak relatively low, while the DEMPC achieves poor performance. Next, the difference between the EMPC-schemes is explored.

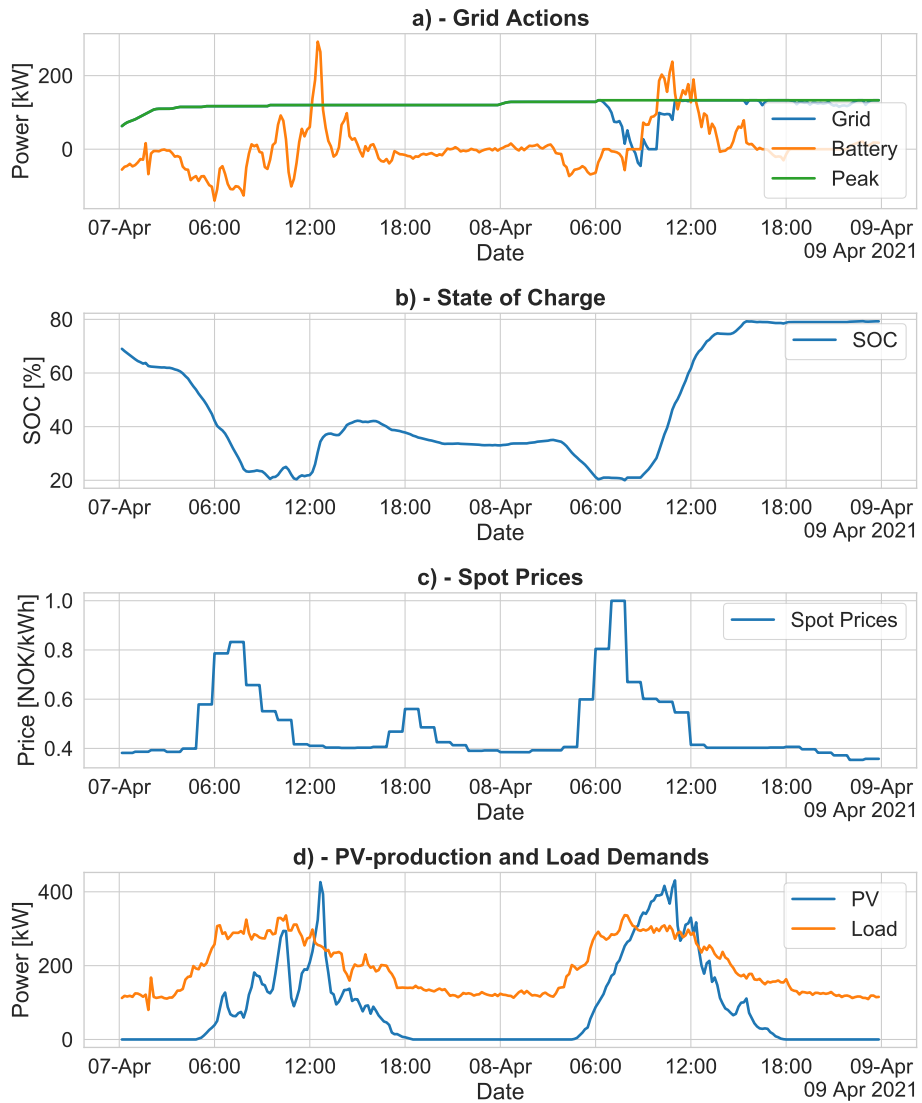


Figure 7.5: Snippet from experiment 3.1 - Effect-based grid tariff and perfect predictions. Grid actions, state of charge, spot-prices, PV-production and Load demands from April 7th to April 9th.

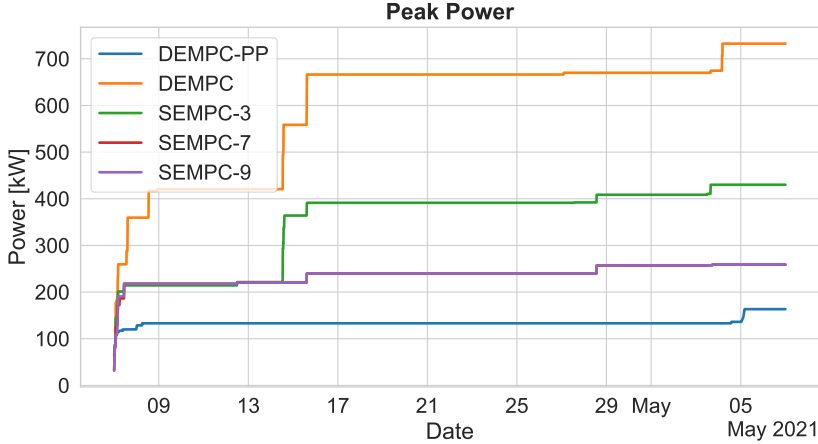


Figure 7.6: Comparison of peak power from April 7th to May 7th.

Figure 7.7 shows the SOC for different EMPC-schemes under uncertainty. The SEMPC follows the same strategy as DEMPC with perfect predictions and uses the battery to avoid the peak around 12.00 on April 12th. However, the next day the SEMPC follows the same pattern, while the other two rely on buying from the grid. DEMPC-PP knows it will cover the load without using the battery significantly, while the DEMPC believes it can do the same. The SEMPC, on the other hand, uses the battery more when the uncertainty is high. By distributing the load between the battery and the grid, the errors corrected by the primary controller have a smaller impact on the peak power. Since the DEMPC-PP does not use the battery to cover the peak on April 13th, the SEMPC’s strategy turned out to be unnecessary in this particular case. However, this conservative behavior shows to be beneficial in the long run.

Figure 7.8 shows the three-hour window from 11.00 to 14.00 on April 7th, which also illustrates the difference between the DEMPC and SEMPC in regards to reducing the peak. The DEMPC is willing to operate closer to the current peak and buys as much power as possible to charge the battery. However, due to a disturbance, the primary controller is forced to buy more energy and push the peak upwards. In contrast, the SEMPC-9 has a more conservative approach, where it does not risk charging the battery and breaking the peak.

The performance of the different EMPC schemes is summarized in Table 7.6. Unlike the same experiment with a fixed tariff (Table 7.4), there are significant differences in operational costs. The main contribution is the maximum power drawn from the grid, which the SEMPCs are better at keeping low, as shown in Figure 7.6. Again this comes at the cost of a higher computational cost, but is well

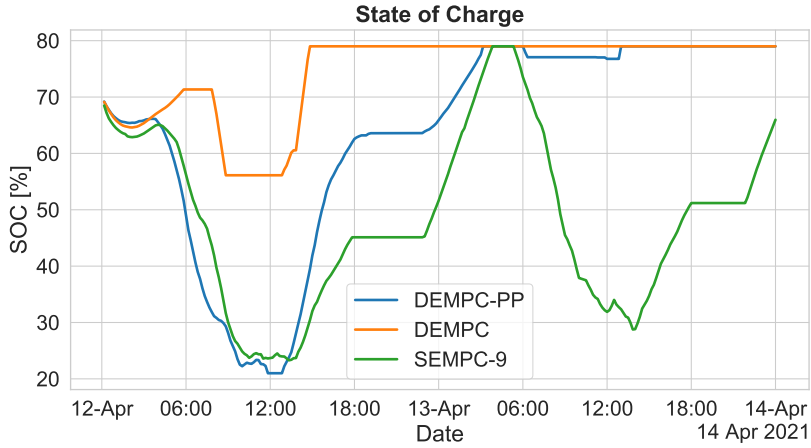


Figure 7.7: Comparison of state of charge for DEMPC with perfect predictions, DEMPC without perfect predictions and SEMPC with 9 branches.

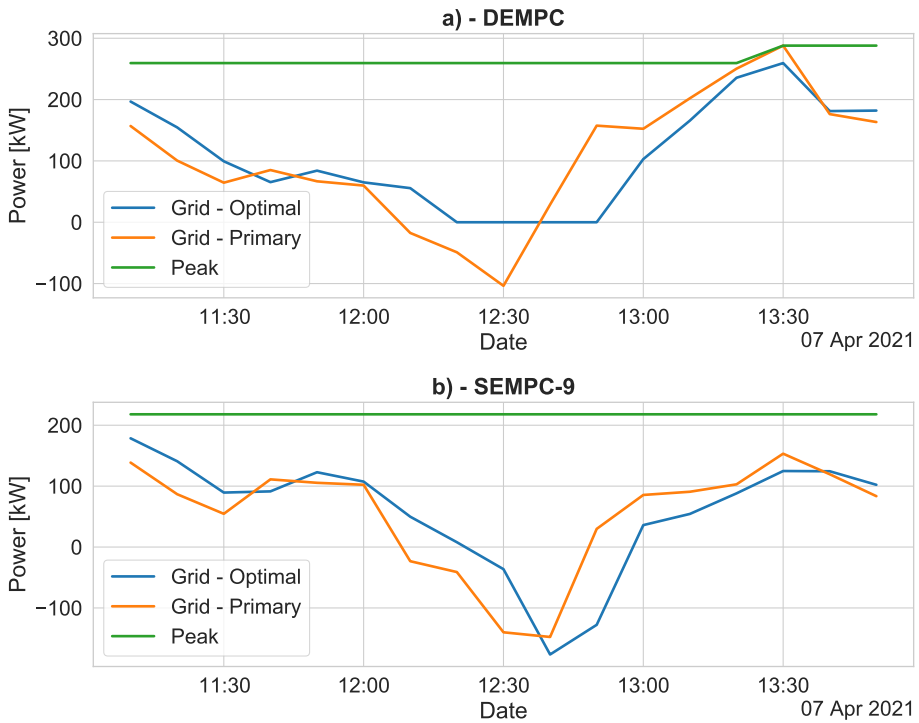


Figure 7.8: Snippet of two hours from 11.00 to 14.00 on April 7th. Grid optimal and grid primary refers to P_G before and after the primary control.

	Operational Costs	Improvement	Average Comp. Time	Worst Case Comp. Time
No Battery	36359 NOK	-	-	-
DEMPC-PP	11275 NOK	69.0%	0.049s	0.118s
DEMPC	40903 NOK	-12.5%	0.049s	0.118s
SEMP-3	25526 NOK	29.8%	0.156s	0.372s
SEMP-7	16701 NOK	54.1%	0.390s	0.995s
SEMP-9	16711 NOK	54.0%	0.542s	1.01s

Table 7.6: Comparison of the different EMPC-schemes with effect-based tariff. DEMPC with perfect predictions is used as benchmark for percentages.

within a reasonable real-time demand.

Discussion

This section revisits the research questions presented in the introduction (Chapter 1).

1. Which methods should be used to efficiently forecast solar production and load demands?
2. What is the value of using an EMPC-scheme as an energy management system at the Skagerak EnergyLab in contrast to more rule-based control strategies?
3. What are the consequences of uncertainties in the EMPC-scheme, and can a robust/stochastic formulation increase the performance?

These questions will be discussed in light of the utilized methods and achieved results obtained and presented in this thesis.

8.1 Forecasting

The objective of forecasting the time series P_{PV} and P_L was to use them in an MPC scheme, and it was therefore focused on keeping computational time low and minimizing errors of the near future prediction. The method of weighing the measurement of the prediction of the near future time steps significantly reduced the one-step error. It was implemented using linear weights, and this method could be improved further, for example, by using ARIMA models that better utilize high auto-correlations. However, ARIMA models introduce more computational complexity and are therefore not used in this thesis.

P_{PV} and P_L are quite different time-series. PV production is dependent on solar radiation, which can give significant and sudden changes on cloudy days. On

the other hand, P_L is dependent on the behavior of the users of the Skagerak Energy Lab. This caused the need for two different prediction methods.

One of the challenges of developing the prediction methods was the lack of data since only data from mid-March to the beginning of May was available. Load demands and PV power generation will likely differ between summer and winter, which the prediction methods should handle. For P_{PV} , the idea of using multiple linear regression (MLR) was to learn the relationship between the weather and production. The weather predictions are updated throughout the year, and the method should, therefore, still be accurate. However, since the MLR was trained in the same season it was tested, it may not be sufficiently accurate when applied to other seasons. Other factors may also affect PV production, for example, if snow covers the cells during winter.

The seasonal argument also follows for load forecasting. It was therefore proposed using a rolling prediction method that collects the previous three weeks. However, three weeks was only used due to lack of data, and taking into account several weeks for predictions may improve the accuracy.

8.2 The Value of EMPC in Skagerak Energylab

The results compared the performance of the EMPC-scheme with a no-battery controller for both fixed grid tariff (Experiment 2.1) and effect-based tariff (Experiment 3.1). This comparison showed that efficient use of the battery leads to significantly lower operational cost for both tariffs when using perfect predictions, compared to selling and buying energy in the moment. However, the alternative to using EMPC as an energy management system is not necessarily no controller nor battery, but rather some less complex control algorithm.

Furthermore, the introduction of uncertainties complicated the control. For the fixed tariff, the EMPC scheme is efficient and much cheaper than a no-battery controller. However, by modeling the effect-based tariff, ignoring uncertainty handling, the operational costs increase compared to the no-battery controller. This is because the DEMPC operates close to the peak, and the uncertainties push it upwards, ultimately reaching a higher peak value than the no-battery controller. This results from our choice in recourse action, where the grid is used to correct the disturbances. A different primary controller can be used, for example, the battery storage system, for correcting the power imbalance.

Also, our models for battery degradation and dynamics are simplified, because they are assumed linear, and parameters are assumed known. However, a model-plant mismatch between the battery model and plant can be expected and affect the performance of the controllers. If the mismatch is small, it may be mitigated by the feedback control in the MPC. However, if there is a significant drop in performance,

the scenario-tree formulation may be extended to include parameters uncertainties. Furthermore, with more data on the battery, a more realistic degradation model can be developed.

8.3 Uncertainties

The consequences of having uncertainties in the EMPC-schemes variate depending on the two price models for grid tariff. For the fixed grid tariff, the consequence of uncertainties was minor. Compared to the upper benchmark, DEMPC-PP, none of the EMPC-schemes were significantly more expensive. Although the effective disturbance can be high, the added cost of buying energy at the wrong time is not severe enough to substantially affect the total cost. Also, the SEMPC-schemes are more robust, but the recourse action ensures no constraint violations and is therefore not strictly necessary. However, in an island-mode configuration of the micro-grid, or if only using the battery as the primary controller, the robustness of the SEMPC could be beneficial.

The behavior of the controller changed when using the effect-based tariff. As already discussed, the DEMPC performs worse than the no-battery controller. In contrast, the SEMPC is efficient in minimizing the peak due to the robustness of the controller. The robust scenarios in Chapter 6.4 cover much of the uncertainty in the predictions \hat{P}_{PV} and \hat{P}_L . In experiment 3.2, two examples of conservative behaviour of the SEMPC is shown. Furthermore, the scenarios were weighted based on the time-of-day. This allowed the controller to stay conservative in periods with high uncertainty, while resembling a DEMPC by trusting predictions more in periods with low uncertainty. The weights are calculated on the training set, which is limited in its time-span. The weights should, therefore, be re-calculated to reflect the uncertainty throughout the year. Overall, this method combines the abilities of deterministic EMPC and robust MPC, which gives good performance on minimizing peak power, without increasing other operational costs significantly.

Conclusion

This thesis has presented a robust scenario-tree economic model predictive control scheme that effectively minimizes the grid peak values when running simulations on real data from Skagerak Energylab. The controller should be able to operate in real-time on the micro-grid because the worst-case computational time is well within the sampling time. The fast performance was achieved by using prediction techniques that are computationally efficient and keeping the complexity of the scenario-tree EMPC low.

A literature study was performed discussing the energy situation in Norway and globally, with a focus on the different challenges that need to be addressed to reduce greenhouse gas emissions. Globally, most of the emissions originate from energy production, which calls for more renewable energy sources. On the other hand, in Norway, reducing emissions is mainly solved by an increase in electrification. This will lead to larger power consumption, which will lead to higher pressure on a limited power grid. A possible solution to both these challenges is micro-grids, which enable distributed energy production. A short intro to the Skagerak EnergyLab micro-grid, the case study used in this thesis, was presented. Further, the economics of being part of the central power grid was discussed and the implication of a future effect-based tariff. Then followed a literature study with the recent economic model predictive control (EMPC) successes in a micro-grid operation.

The following section went into detail about micro-grids before theory on both time-series analysis and model predictive control was presented. In Chapter 6 a mathematical model for the Skagerak micro-grid was developed, and analyses of real data were done to forecast power produced from PV-cells and load demands. This was followed by a thorough examination of the forecast errors or uncertainties that remained in the system. These were incorporated into the control scheme as scenarios, resulting in a scenario-tree EMPC. Finally, the results were presented in Chapter 7.

The key findings from the thesis work are summarized below:

- A robust scenario-tree EMPC is efficient in minimizing peak power, which leads to more efficient use of the power infrastructure.
- Efficiently using the battery with an EMPC-scheme can reduce operational costs compared to a no-battery controller.
- Using a DEMPC without uncertainty handling and modeling of peak power resulted in increased operational costs compared to a non-battery controller.
- The new effect-based grid tariff encourages more sustainable and economical use of the power grid. If the control system is able to keep the peak power low, the new tariff can reduce operational costs.

9.1 Further work

For further research, it would be of great interest to look into the following:

- This thesis handling of uncertainties and scenario selection was done primarily to keep the computational cost low while achieving acceptable performance. This is, however, a wide field of research, and there are methods where the controller better includes the probability distribution of uncertainty in a scenario-tree EMPC.
- The prediction algorithms presented in this work were trained on three weeks of data and then tested on a month. As weather and seasons change, the solutions found are not necessarily as effective. More data and rigorous testing should therefore be done on the system.
- To test if the system performs in real-life, it can be implemented on the Skagerak EnergyLab. Collecting data from a test period could give interesting information that can be used to improve the system further.
- The control system developed in this thesis was fast, so decreasing the sampling time should be possible. This could give an increase in performance.
- Using the battery as a primary controller can be another interesting approach to reduce peak power.

Bibliography

- Andersson, J., Åkesson, J. & Diehl, M. (2012), Casadi: A symbolic package for automatic differentiation and optimal control, Vol. 87.
- Andresen, B. (2021), ‘Over halvparten av nye personbiler er elbiler’.
URL: <https://www.ssb.no/transport-og-reiseliv/artikler-og-publikasjoner/over-halvparten-av-nye-personbiler-er-elbiler>
- Angeli, D., Amrit, R. & Rawlings, J. B. (2012), ‘Economic Model Predictive Control’, *IEEE Transactions on Automatic Control* **57**(7), 1615–1625.
- Bao, J. & Lee, P. L. (2007), Dissipativity and Passivity, in ‘Process Control: The Passive Systems Approach’, Springer London, London, pp. 5–41.
- Berg, K., Resch, M., Weniger, T. & Simonsen, S. (2021), ‘Economic evaluation of operation strategies for battery systems in football stadiums: A Norwegian case study’, *Journal of Energy Storage* **34**(January), 102190.
URL: <https://doi.org/10.1016/j.est.2020.102190>
- Bordons, C., Garcia-Torres, F. & Ridao, M. (2020), *Model Predictive Control of Microgrids*, Springer International Publishing, Springer Nature Switzerland AG.
- Box, G. E. P. & Jenkins, G. (1990), *Time Series Analysis, Forecasting and Control*, Holden-Day, Inc.
- Brown, R. G. & Hwang, P. Y. C. (2012), *Introduction to Random Signals and Applied Kalman Filtering 4th-edition*, John Wiley & Sons, Inc.
- Carli, R., Cavone, G., Pippia, T., Schutter, B. D. & Dotoli, M. (2020), A robust mpc energy scheduling strategy for multi-carrier microgrids, pp. 152–158.
- Chen, B., Lin, P., Lai, Y., Cheng, S., Chen, Z. & Wu, L. (2020), ‘Very-short-term power prediction for PV power plants using a simple and effective RCC-LSTM model based on short term multivariate historical datasets’, *Electronics (Switzerland)* **9**(2).

- Chen, H., Cong, T. N., Yang, W., Tan, C., Li, Y. & Ding, Y. (2009), ‘Progress in electrical energy storage system: A critical review’, *Progress in Natural Science* **19**(3), 291–312.
URL: <https://www.sciencedirect.com/science/article/pii/S100200710800381X>
- CINELDI (2020), ‘Centre for intelligent electricity distribution’.
URL: <https://www.sintef.no/projectweb/cineldi/about/>
- Clarke, W., Manzie, C. & Brear, M. (2016), An economic mpc approach to micro-grid control, pp. 276–281.
- Cominesi, S. R., Farina, M., Giulioni, L., Picasso, B. & Scattolini, R. (2018), ‘A Two-Layer Stochastic Model Predictive Control Scheme for Microgrids’, *IEEE Transactions on Control Systems Technology* **26**(1), 1–13.
- Diehl, M., Amrit, R. & Rawlings, J. B. (2011), ‘A Lyapunov Function for Economic Optimizing Model Predictive Control’, **56**(3), 703–707.
- Ellis, M., Durand, H. & Christofides, P. D. (2014), ‘A tutorial review of economic model predictive control methods’, *Journal of Process Control* **24**(8), 1156–1178.
- Engels, J., Claessens, B. & Deconinck, G. (2020), ‘Optimal combination of frequency control and peak shaving with battery storage systems’, *IEEE Transactions on Smart Grid* **11**(4), 3270–3279.
- ENTSOE (2019), ‘Fast frequency reserve—solution to the nordic inertia challenge’.
- Faulwasser, T., Grüne, L. & Müller, M. A. (2018), ‘Economic nonlinear model predictive control’, *Foundations and Trends in Systems and Control* **5**(1), 1–98.
- Gros, S. & Diehl, M. (2017), ‘Numerical Optimal Control’, **2017**.
- Hans, C. A., Sopasakis, P., Bemporad, A., Raisch, J. & Reincke-Collon, C. (2015), Scenario-based model predictive operation control of islanded microgrids, *in* ‘2015 54th IEEE Conference on Decision and Control (CDC)’, pp. 3272–3277.
- Hans, C. A., Sopasakis, P., Raisch, J., Reincke-Collon, C. & Patrinos, P. (2018), ‘Risk-averse model predictive operation control of islanded microgrids’, *arXiv (Cdc)*, 3272–3277.
- Heirung, T. A. N., Paulson, J. A., O’Leary, J. & Mesbah, A. (2018), ‘Stochastic model predictive control — how does it work?’, *Computers and Chemical Engineering* **114**, 158–170.
URL: <http://dx.doi.org/10.1016/j.compchemeng.2017.10.026>
- Heitsch, H. & Römich, W. (2003), ‘Scenario reduction in stochastic programming’, *Mathematical Programming* **95**(3), 493–511.
- Hicks, G. A. & Ray, W. (1971), ‘Approximation methods for optimal control synthesis’, *Canadian Journal of Chemical Engineering* **49**, 522–528.

- Hoel, N. (2020), ‘Data-driven mpc of microgrid operation, specialization thesis’, *Norwegian University of Science and Technology* .
- Husefest, T. (2020), ‘Data-driven mpc of microgrid operation, specialization thesis’, *Norwegian University of Science and Technology* .
- Junior, A. C. B. (2016), Dynamical modeling and simulation of pv-solar pannels, Vol. 7, pp. 16–23.
- Kayri, M., Kayri, I. & Gencoglu, M. T. (2017), ‘The performance comparison of Multiple Linear Regression, Random Forest and Artificial Neural Network by using photovoltaic and atmospheric data’, *2017 14th International Conference on Engineering of Modern Electric Systems, EMES 2017* pp. 1–4.
- Khodadoost Arani, A. A. & Gharehpetian, G. B. (2014), Enhancement of microgrid frequency control subsequent to islanding process using flywheel energy storage system, in ‘2014 Smart Grid Conference (SGC)’, pp. 1–6.
- Klintberg, E., Dahl, J., Fredriksson, J. & Gros, S. (2016), ‘An improved dual Newton strategy for scenario-tree MPC’, *2016 IEEE 55th Conference on Decision and Control, CDC 2016 (Cdc)*, 3675–3681.
- Klintberg, E. & Gros, S. (2017), ‘A Parallelizable Interior Point Method for Two-Stage Robust MPC’, *IEEE Transactions on Control Systems Technology* **25**(6), 2087–2097.
- Koch, A., Berberich, J. & Allgöwer, F. (2020), ‘Provably robust verification of dissipativity properties from data’, *arXiv* pp. 1–13.
- Krishnamoorthy, D., Foss, B. & Skogestad, S. (2018), ‘A Distributed Algorithm for Scenario-based Model Predictive Control using Primal Decomposition*’, *IFAC-PapersOnLine* **51**(18), 351–356.
URL: <https://doi.org/10.1016/j.ifacol.2018.09.325>
- Krishnamoorthy, D., Thombre, M., Skogestad, S. & Jäschke, J. (2018), ‘Data-driven scenario selection for multistage robust model predictive control’, *IFAC-PapersOnLine* **51**(20), 462–468. 6th IFAC Conference on Nonlinear Model Predictive Control NMPC 2018.
URL: <https://www.sciencedirect.com/science/article/pii/S2405896318327046>
- Kumar, R., Jalving, J., Wenzel, M. J., Ellis, M. J., ElBsat, M. N., Drees, K. H. & Zavala, V. M. (2019), ‘Benchmarking stochastic and deterministic MPC: A case study in stationary battery systems’, *AIChE Journal* **65**(7), 1–16.
- Labeeuw, W. & Deconinck, G. (2013), ‘Residential electrical load model based on mixture model clustering and markov models’, *IEEE Transactions on Industrial Informatics* **9**(3), 1561–1569.

- Laresgoiti, I., Käbitz, S., Ecker, M. & Sauer, D. U. (2015), ‘Modeling mechanical degradation in lithium ion batteries during cycling: Solid electrolyte interphase fracture’, *Journal of Power Sources* **300**, 112–122.
URL: <https://www.sciencedirect.com/science/article/pii/S0378775315302949>
- Marnay, C., Chatzivasileiadis, S., Abbey, C., Iravani, R., Joos, G., Lombardi, P., Mancarella, P. & Von Appen, J. (2015), ‘Microgrid evolution roadmap’, *Proceedings - 2015 International Symposium on Smart Electric Distribution Systems and Technologies, EDST 2015* pp. 139–144.
- Mayne, D. (2016), ‘Robust and stochastic model predictive control: Are we going in the right direction?’, *Annual Reviews in Control* **41**, 184–192.
- Mayne, D. Q., Rawlings, J. B., Rao, C. V. & Scokaert, P. O. (2000), ‘Constrained model predictive control: Stability and optimality’, *Automatica* **36**(6), 789–814.
- Moghram, I. & Rahman, S. (1989), ‘Analysis and Evaluation of Five Short-Term Load Forecasting Techniques’, *IEEE Power Engineering Review* **9**(11), 42–43.
- Nocedal, J., Andreas, W. & Richard, W. (2008), ‘Adaptive barrier update strategies for nonlinear interior methods’.
- Nocedal, J. & Wright, S. J. (2006), *Numerical Optimization*.
- Novickij, I. & Joos, G. (2019), Model predictive control based approach for microgrid energy management, pp. 1–4.
- NVE (2018), ‘Høring - forslag til endringer i forskrift om kontroll av nettvirksomhet - tariffer’.
URL: <https://www.nve.no/om-nve/regelverk/forskriftsendringer-pa-horing/horing-forslag-til-endringer-i-forskrift-om-kontroll-av-nettvirksomhet-tariffer-avsluttet/>
- Olivares, D. E., Mehrizi-Sani, A., Etemadi, A. H., Cañizares, C. A., Iravani, R., Kazerani, M., Hajimiragha, A. H., Gomis-Bellmunt, O., Saeedifard, M., Palma-Behnke, R., Jiménez-Estévez, G. A. & Hatziargyriou, N. D. (2014), ‘Trends in microgrid control’, *IEEE Transactions on Smart Grid* **5**(4), 1905–1919.
- Pandas, D. T. (2020), ‘Pandas data analysis package’.
URL: <https://doi.org/10.5281/zenodo.3509134>
- Paris Agreement* (2015).
URL: https://treaties.un.org/pages/ViewDetails.aspx?src=TREATY&mtdsg_no=XXVII-7-d&chapter=27&clang=en
- Parisio, A., Rikos, E. & Glielmo, L. (2014), ‘A model predictive control approach to microgrid operation optimization’, *IEEE Transactions on Control Systems Technology* **22**(5), 1813–1827.

- Patiño, J., Márquez, A. & Espinosa, J. (2014), An economic mpc approach for a microgrid energy management system, *in* ‘2014 IEEE PES Transmission Distribution Conference and Exposition - Latin America (PES T D-LA)’, pp. 1–6.
- Pedregosa, F., Varoquaux, G., Gramfort, A., Michel, V., Thirion, B., Grisel, O., Blondel, M., Prettenhofer, P., Weiss, R., Dubourg, V., Vanderplas, J., Passos, A., Cournapeau, D., Brucher, M., Perrot, M. & Duchesnay, E. (2011), ‘Scikit-learn: Machine learning in Python’, *Journal of Machine Learning Research* **12**, 2825–2830.
- Pirkelmann, S., Angeli, D. & Grüne, L. (2019), ‘Approximate computation of storage functions for discrete-time systems using sum-of-squares techniques’, *IFAC-PapersOnLine* **52**(16), 508–513.
- Qin, J. & Badgwell, T. (2003), ‘A survey of industrial model predictive control technology’, *Control engineering practice* **11**, 733–764.
- Rahman, M. M., Oni, A. O., Gemechu, E. & Kumar, A. (2020), ‘Assessment of energy storage technologies: A review’, *Energy Conversion and Management* **223**, 113295.
URL: <https://www.sciencedirect.com/science/article/pii/S0196890420308347>
- Raković, S. V. (2019), *Robust Model Predictive Control*, Springer London, London, pp. 1–11.
URL: https://doi.org/10.1007/978-1-4471-5102-9_2-3
- Rawlings, J. B. & Amrit, R. (2009), Optimizing Process Economic Performance Using Model Predictive Control, *in* ‘Nonlinear Model Predictive Control: Towards New Challenging Applications’, Springer Berlin Heidelberg, pp. 119–138.
- Regjeringen.no (2016), ‘Power supply and the electricity grid’.
URL: <https://www.regjeringen.no/en/topics/energy/the-electricity-grid/power-supply-and-the-electricity-grid/id2353792/>
- Ritchie, H. (2021), ‘Electricity mix’.
URL: <https://ourworldindata.org/electricity-mix>
- Sandelic, M., Stroe, D.-I. & Iov, F. (2018), ‘Battery storage-based frequency containment reserves in large wind penetrated scenarios: A practical approach to sizing’, *Energies* **11**(11).
URL: <https://www.mdpi.com/1996-1073/11/11/3065>
- Scherer, C. & Weiland, S. (2020), ‘Linear Matrix Inequalities in Control Problems’, *Differential Equations* **56**(11), 1496–1501.
- Shan, Y., Hu, J., Li, Z. & Guerrero, J. M. (2018), ‘A model predictive control for renewable energy based ac microgrids without any pid regulators’, *IEEE Transactions on Power Electronics* **33**(11), 9122–9126.

- Solcast (2021), ‘Solar irradiance data’.
URL: <https://solcast.com/>
- Statistics, N. (2020), ‘Electricity’.
URL: <https://www.ssb.no/en/natur-og-miljo/statistikker/klimagassn>
- Statistics, N. (2021), ‘Emissions to air’.
URL: <https://www.ssb.no/en/energi-og-industri/energi/statistikk/elektrisitet>
- Vetter, J., Novák, P., Wagner, M., Veit, C., Möller, K.-C., Besenhard, J., Winter, M., Wohlfahrt-Mehrens, M., Vogler, C. & Hammouche, A. (2005), ‘Ageing mechanisms in lithium-ion batteries’, *Journal of Power Sources* **147**(1), 269–281.
URL: <https://www.sciencedirect.com/science/article/pii/S0378775305000832>
- Villalva, M. G., Gazoli, J. R. & Filho, E. R. (2009), ‘Comprehensive approach to modeling and simulation of photovoltaic arrays’, *IEEE Transactions on Power Electronics* **24**(5), 1198–1208.
- Vinod, Kumar, R. & Singh, S. (2018), ‘Solar photovoltaic modeling and simulation: As a renewable energy solution’, *Energy Reports* **4**, 701–712.
URL: <https://www.sciencedirect.com/science/article/pii/S2352484718300842>
- Virtanen, P., Gommers, R., Oliphant, T. E., Haberland, M., Reddy, T., Cournapeau, D., Burovski, E., Peterson, P., Weckesser, W., Bright, J., van der Walt, S. J., Brett, M., Wilson, J., Millman, K. J., Mayorov, N., Nelson, A. R. J., Jones, E., Kern, R., Larson, E., Carey, C. J., Polat, İ., Feng, Y., Moore, E. W., VanderPlas, J., Laxalde, D., Perktold, J., Cimrman, R., Henriksen, I., Quintero, E. A., Harris, C. R., Archibald, A. M., Ribeiro, A. H., Pedregosa, F., van Mulbregt, P. & SciPy 1.0 Contributors (2020), ‘SciPy 1.0: Fundamental Algorithms for Scientific Computing in Python’, *Nature Methods* **17**, 261–272.
- Wächter, A. (2009), *Short Tutorial: Getting Started With Ipopt in 90 Minutes*, number 09061 in ‘Dagstuhl Seminar Proceedings’, Schloss Dagstuhl - Leibniz-Zentrum fuer Informatik, Germany, Dagstuhl, Germany.
URL: <http://drops.dagstuhl.de/opus/volltexte/2009/2089>
- Wächter, A. & Biegler, L. (2005), ‘On the implementation of an interior-point filter line-search algorithm for large-scale nonlinear programming.’.
- Zhou, H., Hans, C. A. & Zhang, W. (2016), Minimax model predictive operation control of grid-connected microgrids, in ‘2016 IEEE Conference on Control Applications (CCA)’, pp. 58–63.

Appendix

A.1 Software and Solver

In this thesis, the software tool CasADi (Andersson et al. 2012) has been used for the implementation and simulation of the system. CasADi is an open source tool offering a symbolic framework for setting up and solving numerical optimization. CasADi comes with several different solvers for the optimization and in this thesis the IPOPT solver has been used. The explanation given here is based on Nocedal & Wright (2006) and some of the IPOPT documentation, Wächter & Biegler (2005), Wächter (2009), Nocedal et al. (2008). IPOPT is an interior point line search filter method for nonlinear programming problems. The algorithm considers the problem formulated as in A.1. IPOPT introduces slack variables to transform the inequality constraints into equality constraints.

$$\begin{aligned}
 & \min_{x,s} f(x) \\
 & \text{s.t.} \\
 & c_E(x) = 0, \\
 & c_I(x) - s = 0, \\
 & s \geq 0
 \end{aligned} \tag{A.1}$$

A.1.1 Interior Points methods

Interior point methods, also known as barrier methods is the main component in the IPOPT algorithm. A barrier problem is formulated as [A.2], with μ as the barrier parameter. IPOPT reformulates it into a primal-dual method, by applying Newton's method to the KKT conditions.

$$\begin{aligned}
\min_{x,s} \quad & f(x) - \mu \sum \ln(s_i) \\
\text{s.t.} \quad & \\
& c_E(x) = 0, \\
& c_I(x) - s = 0,
\end{aligned} \tag{A.2}$$

A.1.2 Line Search

To decide the step length, line search is used. Line search methods finds a step length from the current point that results in a next point (sufficiently) closer to the optimal solution. IPOPT uses a Newton-type method to find the direction of the next step.

A.1.3 Filters

After finding where the next step should be taken, the new point must be evaluated to see if it did bring the algorithm closer to the optimal solution. Here IPOPT uses a method called filters, where a multi objective problem is evaluated. The problem consist of two objective functions, one is the objective function from the original problem and the other is the norm of the constraints. The filter ensures that a step decreases either the objective function or the norm of the constraints.